Mechano-regulation of GLP-1 production by Piezo1 in intestinal L cells

Yanling Huang[1#], Haocong Mo[1#], Jie Yang[2#], Luyang Gao[1#], Tian Tao[1], Qing Shu[1], Wenying Guo[1], Yawen Zhao[1], Jingya Lyu[1], Qimeng Wang[3], Jinghui Guo[4], Hening Zhai[5], Linyan Zhu[6], Hui Chen[3*], Geyang Xu[1,7*]

[1]Department of Physiology, School of Medicine, Jinan University, 601 Huangpu Avenue West, Tianhe District, Guangzhou 510632, Guangdong, China;

[2]Department of Pathology, School of Basic Medicine, Guangzhou Medical University, Guangzhou 511436, Guangdong, China;

[3]Biotherapy Center, Cell-gene Therapy Translational Medicine Research Center, the Third Affiliated Hospital, Sun Yat-Sen University, Guangzhou 510630, Guangdong, China.

[4]School of Medicine, The Chinese University of Hong Kong, Shenzhen 518172, Guangdong, China;

[5]Endoscopy Center, The First Affiliated Hospital of Jinan University, 613 Huangpu Avenue West, Tianhe District, Guangzhou 510630, Guangdong, China;

[6]Department of Pharmacology, School of Medicine, Jinan University, Guangzhou 510632, Guangdong, China.

[7]Key Laboratory of Viral Pathogenesis & Infection Prevention and Control (Jinan University), Ministry of Education, Guangzhou 510632, Guangdong, China.

[#]Yanling Huang, Haocong Mo, Jie Yang and Luyang Gao contributed equally to this work.

* Corresponding Author:
Geyang Xu
Department of Physiology, School of Medicine, Jinan University, 601 Huangpu Avenue West, Tianhe District, Guangzhou, Guangdong, 510632, China.
Tel: 86-20-85220260
Fax: 86-20-85221343
E-mail: xugeyangliang@163.com

Or

Hui Chen
Biotherapy Center; Cell-Gene Therapy Translational Medicine Research Center, the Third Affiliated Hospital of Sun Yat-Sen University, Guangzhou 510630, Guangdong, China.
Tel: 86-20-85252826
E-mail: chenh567@mail.sysu.edu.cn

Abstract

Glucagon-like peptide 1 (GLP-1) is a gut-derived hormone secreted by intestinal L cells and vital for postprandial glycemic control. As open-type enteroendocrine cells, whether L cells can sense mechanical stimuli caused by chyme and thus regulate GLP-1 synthesis and secretion is unexplored. Our study showed expression of Piezo1 in intestinal L cells. Its level varied in different energy status and correlates with blood glucose and GLP-1 levels. Mice with L cell-specific loss of Piezo1 (*IntL-Piezo1*$^{-/-}$) exhibited impaired glucose tolerance, increased body weight, reduced GLP-1 production and decreased CaMKKβ/CaMKIV-mTORC1 signaling pathway under normal chow diet or high fed diet. Activation of the intestinal Piezo1 by its agonist Yoda1 or intestinal bead implantation increased the synthesis and secretion of GLP-1, thus alleviated glucose intolerance in diet-induced-diabetic mice. Overexpression of Piezo1, Yoda1 treatment or stretching stimulated GLP-1 production and CaMKKβ/CaMKIV-mTORC1 signaling pathway, which could be abolished by knockdown or blockage of Piezo1 in primary cultured mouse L cells and STC-1 cells. These findings suggest a previously undiscovered mechano-regulation of GLP-1 production in L cells, which may shed new light on the treatments of diabetes.

Keywords: Piezo1, Glucagon-like peptide 1, Intestinal L cells, CaMKKβ, CaMKIV, Mammalian target of rapamycin

63 **Abbreviations:**

CaMKKβ	Ca^{2+}/calmodulin-dependent protein kinase kinase β
CaMKIV	Ca^{2+}/calmodulin-dependent protein kinases IV
EECs	Enteroendocrine cells
mTOR	mechanistic target of rapamycin
RYGB	Roux-en-Y gastric bypass
S6K	p70 S6 Kinase
S6	S6 Ribosomal Protein
T2DM	Type 2 Diabetes Mellitus
CCK	Cholecystokinin

64

Introduction

The gastrointestinal (GI) tract represents the largest endocrine organ in the human body. The enteroendocrine cells (EECs) located throughout the GI tract secrete a large number of gastrointestinal hormones to regulate a variety of physiological processes and are key regulators for energy homeostasis (Bany Bakar et al., 2023). GLP-1 is one of the gut-derived peptide hormones essential for postprandial glycemic control (Song et al., 2019). It is produced from Proglucagon (Gcg) by proprotein convertase in the intestinal L cells, a group EECs predominantly situated in the distal gut (Drucker, 2006; Rouillé et al., 1997). The circulating GLP-1 levels rapidly increase after meal and reduce postprandial blood glucose fluctuations by augmenting insulin secretion, suppressing glucagon secretion and slowing gastric emptying (Drucker, 2006; Willms et al., 1996). Nowadays, GLP-1-based therapy is well-recognized and commonly used in treatment of Type 2 Diabetes Mellitus (T2DM) (Saxena et al., 2021; Tan et al., 2022). Although GLP-1 analogs such as exenatide and liraglutide have been approved for clinical use in the treatment of T2DM, these drugs may lead to side effects such as pancreatitis (Elashoff et al., 2011), as well as potential risk of inducing medullary thyroid carcinoma (Bezin et al., 2023). Therefore, elucidation of the mechanism that regulates GLP-1 production is essential for the development of new drug targets for the treatment of diabetes.

EECs can be divided into two categories according to its morphology: open type and closed type. The open type EECs possess microvilli protruding into the gut lumen and have direct contact with the luminal contents. In contrast, the closed type EECs are located basolaterally without direct contact with the lumen (Gribble & Reimann, 2016). Both types of EECs synthesize and store peptides or hormones in secretory granules and release them by exocytosis at the basolateral membrane upon mechanical, chemical or neural stimulation (Atanga et al., 2023). As open-type cells, L cells received both chemical and mechanical signals from the luminal contents, and neural signals from the nerves (Furness et al., 2013). It has been well-documented that nutrients such as glucose, lipids, and amino acids in the intestinal lumen can stimulate

94 the secretion of GLP-1 from L cells (Diakogiannaki et al., 2012). GLP-1 secretion can
95 also be stimulated by intrinsic cholinergic nerves (Anini et al., 2002; Drucker, 2006).
96 However, whether and how L cells coordinate mechanical stimuli from intestinal
97 lumen to regulate GLP-1 production remain poorly understood.

98 Piezo channels, including Piezo1 and Piezo2 have recently been identified as a
99 mechanosensitive ion channel that is involved in the sensation of multiple mechanical
100 stimuli, such as shear stress, pressure, and stretch (Gudipaty et al., 2017; Li et al.,
101 2014; Romac et al., 2018). They allow the influx of cations such as Ca^{2+} and Na^{+} in
102 response to mechanical tension and converts mechanical stimuli into various electrical
103 and chemical signals. Piezo1 plays a crucial role in blood pressure regulation, red
104 blood cell volume regulation, bone homeostasis, pulmonary and cardiac functions
105 (Cahalan et al., 2015; Lai et al., 2022; Wang et al., 2023; Wang et al., 2016). Previous
106 studies have reported that Piezo1 is expressed in the intestinal epithelium, regulating
107 barrier function, mucus secretion, and inflammation (Jiang et al., 2021; Liu et al.,
108 2022; Xu et al., 2021). Interestingly, accumulating evidence demonstrates the
109 regulation of insulin secretion by Piezo1 (Deivasikamani et al., 2019; Ye et al., 2022).
110 Recent studies have also reported that Piezo2 is expressed in a population of EECs
111 and convert force into serotonin release (Alcaino et al., 2018; Treichel et al., 2022).
112 These findings suggest a critical role of Piezo channels in the mechano-regulation of
113 hormone production. However, whether Piezo channels are expressed L cells and play
114 a role in GLP-1 production remain unknown.

115 Here, we present evidence that Piezo1 channels on intestinal L cells mediate the
116 mechanosensing from intestinal contents and trigger the synthesis and secretion of
117 GLP-1 through CaMKKβ/CaMKIV-mTORC1 signaling pathway, thus regulating
118 glucose homeostasis. Our research provides new insights for the treatment of T2DM
119 and a new theoretical basis for hypoglycemic medicines targeting Piezo1.

Materials and Methods

Collection of Human Intestine Samples

Obese participants with type 2 diabetes (n=6, BMI=45.87±4.889 kg/m^2) and one-year post-RYGB patients (n=6, BMI=25.48±1.085 kg/m^2) were recruited in current study. Written informed consent was obtained from each donor. The study protocol was approved by the Institutional Review Board of Jinan University. Mucosal biopsies were obtained from human intestines by using a colonoscopy (CF-HQ290I; Olympus).

Genetic Mouse Generation

Villin-Flippase (Vil-Flp) mice

Vil-Flp knock-in mouse model was developed by Shanghai Model Organisms Center, Inc. The targeting construct was designed to insert a 2A-Flp-WPRE-pA coexpression cassette into the stop codon of mouse *Vil1* gene via homologous recombination using CRISPR/Cas9 system. 5'-AGCCCCTACCCTGCCTTCAA-3' was chosen as Cas9 targeted guide RNA (sgRNA). The donor vector, sgRNA and Cas9 mRNA was microinjected into C57BL/6J fertilized eggs. F0 generation mice positive for homologous recombination were identified by long PCR. The primers (I-IV) used for detection of the correct homology recombination were I: 5’-ACTTCAGGCCTAACGCTCAC-3’ and II: 5’-TGTCCTGCAGGCAGAGAAAG-3’ for the correct 5’ homology arm recombination, and III: 5’-GTGCCGTCTCTAAGCACAGT-3’and IV: 5’-TGTTGGTGCTTCGGAGTGTT-3’for the correct 3' homology arm recombination. The PCR products were further confirmed by sequencing. F0 mice were crossed with C57BL/6J mice to obtain *Vil-Flp* heterozygous mice.

Flp-dependent Glucagon-Cre (FGC) mice

FGC mouse model was developed by Shanghai Model Organisms Center, Inc. The targeting construct was designed to insert an IRES-F3-Frt-Wpre-pA-Cre-Frt-F3 expression cassette into the 3’ UTR of mouse *Gcg* gene of via homologous recombination using CRISPR/Cas9 system. 5’-ATGCAAAGCAATATAGCTTC-3’

150 was chosen as Cas9 targeted guide RNA (sgRNA). The donor vector, sgRNA and
151 Cas9 mRNA was microinjected into C57BL/6J fertilized eggs. F0 generation mice
152 positive for homologous recombination were identified by long PCR. The primers
153 (I-IV) used for detection of the correct homology recombination were I:
154 5'-TGCTACACAGGAGGTCTGTC-3' and II: 5'-AGGCATGCTCTGCTATCACG-3'
155 for the correct 5' homology arm recombination, and III:
156 5'-CCCTCCTAGTCCCTTCTCAGT-3' and IV:
157 5'-GCCAAGGACATCTTCAGCGA-3' for the correct 3' homology arm
158 recombination. The PCR products were further confirmed by sequencing. F0 mice
159 were crossed with C57BL/6J mice to obtain *FGC* heterozygous mice.

160 *IntL-Cre mice*

161 *Vil-Flp* mice were crossed with *FGC* mice to obtain Intestinal L cell-specific Cre
162 (*IntL-Cre*) mice.

163 *IntL-Piezo1$^{-/-}$ mice*

164 *Piezo1$^{loxp/loxp}$* mice (B6.Cg-Piezo1$^{tm2.1Apat}$/J) purchased from Jackson laboratory
165 were crossed with IntL-Cre mice to generate *IntL-Piezo1$^{-/-}$* mice.

166 PCR is used to identify the genotype of mice during the subsequent mating and
167 breeding process. The primers required for mouse genotyping are shown in the SI
168 Appendix, Table S1.

169

170 **Mouse Validation**

171 *mT/mG* reporter mice were purchased from Shanghai Model Organisms Center,
172 Inc. *IntL-Cre* mice were bred with *mT/mG* reporter mice to further validate Cre
173 recombinase activity and specificity. Every single *IntL-Cre* mouse was confirmed by
174 *mT/mG* reporter mice before breeding with *Piezo1$^{loxp/loxp}$* mice to generate Intestinal L
175 cell-Piezo1$^{-/-}$ (*IntL-Piezo1$^{-/-}$*) mice.

176

177 **Frozen Tissue Confocal Imaging**

178 *IntL-Cre-mT/mG* reporter mice were sacrificed. Fresh ileum and pancreas tissues
179 were collected and embedded in O.C.T. compound for histological analysis
180 immediately. Slices of the tissues were cut for confocal imaging, which was protected
181 from light. Fluorescence was detected by laser scanning confocal microscopy (Li et
182 al., 2022).
183
184 **Animal Housing and Treatment**
185 Male mice were maintained on a 12-hour light/12-hour dark cycle environment.
186 Normal chow diet (NCD) or a high-fat diet (HFD) and water were available ad
187 libitum unless specified otherwise. The animal protocols were approved by the
188 Animal Care and Use Committee of Jinan University.
189 Male *IntL-Piezo1*$^{-/-}$ mice and age-matched control littermates (*Piezo1*$^{loxp/loxp}$,
190 *Vil-Flp*, *FGC*, *IntL-Cre* mice) fed with NCD or HFD were used in the experiments.
191 Male *Piezo1*$^{loxp/loxp}$ and *IntL-Piezo1*$^{-/-}$ mice fed with 10 week-high fat diet were
192 intraperitoneally injected with normal saline (NS) or the GLP-1R agonist Exendin-4
193 (100 ug/kg body weight) for 7 consecutive days.
194 High fat diet induced diabetic mice were randomly divided into 3 groups. When
195 indicated, animals were injected intraperitoneally with Vehicle, Yoda1 (2 μg per
196 mouse) or GsMTx4 (250 μg/kg) for 7 consecutive days.
197 High fat diet treated *IntL-Piezo1*$^{-/-}$ mice were randomly divided into 2 groups.
198 When indicated, animals were injected intraperitoneally with Vehicle, Yoda1 (2 μg per
199 mouse) for 7 consecutive days.
200 Diet induce diabetic C57BL/6J mice were divided into sham and intestinal bead
201 implantation groups.
202
203 **Food and water intake detection**
204 The food and water intake were quantified using metabolic cages (Cat 41853,
205 Ugo Basile, Comerio, Italy). The mice were individually housed in these specialized
206 cages and given a period of 3 days to acclimate before data collection began. They
207 had unrestricted access to food and water, which was continuously monitored

208 throughout the study. The 41850-010 software/interface package, consisting of
209 EXPEDATA (for data analysis) and METASCREEN (for data collection) software,
210 along with the IM-2 interface module, was employed to record and analyze the data.
211
212 **Intraperitoneal Glucose Tolerance Test**
213 Mice were fasted for 12 hours before measuring their fasting glucose levels. An
214 intraperitoneal glucose tolerance test (IPGTT) was performed by administering 1.5
215 g/kg body weight of glucose. Blood glucose concentrations were measured at
216 specified time points using a glucometer by collecting tail vein blood samples.
217
218 **Insulin Tolerance Test**
219 Mice were subjected to a 4-hour fast before measurement of fasting glucose were
220 taken. Insulin tolerance tests (ITT) were conducted with a dose of 0.75 U/kg body
221 weight of insulin. Blood glucose levels were measured at specified time points.
222
223 **Intestinal Bead implantation**
224 High-fat diet-induced type 2 diabetic C57BL/6J mice were fasted 6 to 8 h before
225 the operation. Standard aseptic procedures were used throughout the operation. For
226 bead implantation, a 1cm incision was made on the abdominal wall to expose the
227 intestine. A 1 cm incision was made approximately 1cm above the ileocecal region. A
228 2.5 mm diameter bead was implanted into the ileum of the mouse through an incision.
229 Then the wound was closed with suture. Finally, the abdominal wall was closed with
230 suture. For sham operation, all the procedures were the same as the bead implantation
231 except that the bead was not implanted.
232
233 **Stretching of isolated ileum**
234 About 2cm ileum was isolated from control and *IntL-Piezo1*$^{-/-}$ mice and kept in
235 the specimen chamber filled with Tyrode's solution (KCl 0.2g/L, NaCl 8g/L, $CaCl_2$
236 0.2g/L, $MgCl_2$ 0.1g/L, $NaHCO_3$ 1g/L, NaH_2PO_4 0.05g/L, Glucose 1g/L) of 37°C

237 gassed with oxygen. The specimen was connected to the force transducer of organ
238 bath system (HW200S, Techman, Chengdu, CN). Adjust the transducer to apply
239 traction force of 1.5 grams on the tissue and maintained for two hours.
240
241 **Measurement of GLP-1 Secretion**
242 The measurement of GLP-1 secretion was carried out according to previously
243 described methods (Zhai et al., 2018). Samples were collected in the presence of
244 aprotinin (2 μg/mL), EDTA (1 mg/mL) and diprotin A (0.1 mmol/L), and stored at
245 -80 °C before use. GLP-1 levels were assayed using enzyme immunoassay kits
246 following the manufacturer's instructions.
247
248 **Histological Analysis**
249 Tissues were collected, fixed with 4% paraformaldehyde, embedded in paraffin,
250 and cut into 4μm sections. Standard protocols were followed for staining the sections
251 with hematoxylin-eosin. Photomicrographs were captured under an inverted
252 microscope (Leica, Germany).
253
254 **Immunofluorescence**
255 Paraffin sections were dewaxed and rehydrated. After antigen retrieval in citrate
256 buffer (pH6.0), sections were blocked with normal serum and then incubated with
257 rabbit anti-Piezo1 (1:400) and mouse anti-GLP-1 (1:500) antibodies at 4°C overnight.
258 The sections were then incubated with a mixture of secondary antibodies. Images
259 were taken by laser scanning confocal microscopy (Leica SP8). Fluorescence
260 intensity was quantitated by ImageJ software.
261
262 **In situ hybridization**
263 Paraffin sections were dewaxed and rehydrated. After antigen retrieval in in citrate
264 buffer (pH6.0), the sections were incubated with Proteinase K (5ug/ml) at 37°C for
265 the 15 minutes. Then the sections were hybridized with the probes overnight in a

266 temperature-controlled chamber at 40°C. The Piezo1 probe sequences were as follows:
267 5′-CTGCAGGTGGTTCTGGATATAGCCC-3’,5′-AAGAAGCAGATCTCCAGCCCG
268 AAT-3’, 5′-GCCATGGATAGTCAATGCACAGTGC-3’. After washing with SSC
269 buffers, the sections were hybridized in pre-warmed branch probes at 40°C for 45
270 minutes. After washing with SSC buffers, the sections were hybridized with signal
271 probe at 42°C for 3 hours. After washing with SSC buffers, the sections were blocked
272 with normal serum and then incubated with mouse anti-GLP-1 (1:500) antibody at
273 4°C overnight followed by secondary antibody. Images were taken laser scanning
274 confocal microscopy (Leica SP8) and the fluorescence signals were quantified by
275 ImageJ.
276
277 **Western Blot Analysis**
278 Tissues and cells were harvested. Ileal mucosa was scraped for protein extraction.
279 Protein extraction was performed by using RIPA lysis buffer (50mM Tris PH 7.4,
280 150mM NaCl, 1% Triton X-100, 0.1% SDS, 1% Sodium deoxycholate, 1mM PMSF
281 and protease inhibitor cocktail.), then 40 μg of proteins were loaded onto an
282 SDS-PAGE gel for separation. After the separation, the proteins were transferred onto
283 a nitrocellulose membrane. The membrane was then incubated in blocking buffer at
284 room temperature for 1 hour. For overnight incubation, the membrane and primary
285 antibody (at the recommended dilution as stated in the product datasheet) were
286 immersed in primary antibody dilution buffer, with gentle agitation, at 4°C.
287 Subsequently, the membrane was incubated with a secondary antibody that
288 specifically recognizes and binds to the primary antibody. Finally, Western blotting
289 luminol reagent was used to visualize bands. The grey scale values of the bands were
290 measured using ImageJ software.
291

292 **RNA extraction, quantitative real-time PCR**

293 RNA was extracted and reverse-transcribed into cDNAs using RT-PCR kit.
294 Real-time PCR was performed as previously described (Zhai et al., 2018). Sequences
295 for the primer pairs used in this study were shown in SI Appendix, Table S2.

296

297 **Isolation of Mouse Intestinal L Cells**

298 A 5~6cm long ileum segment was collected from the IntL-cre-mT/mG mouse. The
299 tissue was washed with ice-cold PBS twice to remove the chyme in the lumen. The
300 tissue was minced into 0.5mm^3 pieces in ice-cold PBS and then digested in 100mIU
301 collagenase I and 0.01g/mL trypsin at 37°C for 30min with rotation. After digested
302 tissue was passed through 40μm and 30μm cell strainers sequentially, then centrifuged
303 for 7min at 4°C. The cell pellete was resuspended in red cell lysis buffer and
304 incubated for 10min at room temperature. The unlysed cells were collected by
305 centrifugation and resuspended with 1mL cold PBS. The GFP positive cells was
306 sorted by fluorescence-activated cell sorting (FASC) on Beckman Coulter MoFlo
307 XDP cell sorter system.

308

309 **Cell Culture and Treatments**

310 STC-1 cells were maintained in DMEM medium supplemented with 2.5% fetal
311 bovine serum and 10% equine serum at 37 °C with 5% CO_2 air. L cells were
312 maintained in DMEM medium supplemented with 10% fetal bovine serum.

313 For cell transfection, cells were plated at optimal densities and grown for 48 h.
314 Cells were then transfected with GFP, Piezo1-GFP, CaMKKβ, CaMKIV by using
315 lipofectamine reagent according to the manufacturer's instructions.

316 For stable knockdown of Piezo1 in STC-1 cells, short hairpin RNA (shRNA)
317 sequences for mouse Piezo1 interference were cloned in to pLKO.1 vector. To
318 produce lentivirus, psPAX2, pMD2G and pLKO.1 or pLKO.1-shPiezo1 plasmids
319 (siPiezo1: CCAACCTTATCAGTGACTT) were co-transfected into 293T cells with
320 lipofectamine 2000 reagent. Supernatant containing lentivirus was collected 48 hours

321 after transfection and filtered through 0.45μm filter. The virus-containing supernatant
322 was used to infect STC-1 cells. Forty-eight hours after infection, the STC-1 cells were
323 subjected to 1ug/mL puromycin selection for 2-3 days.
324 For cell stretching, cells were grown in silicone elastic chambers coated by 0.1 %
325 gelatin solution. After incubated at 37 °C for 24-48 hours, The chambers were
326 subjected to mechanical stretch to 120% of their original length.
327
328 **Calcium Imaging**
329 Cells were plated onto confocal dishes at optimal densities and grown for 24 h.
330 Cells were loaded with the calcium fluorescent probe fluo-4 AM (1 μM) for 1 h at
331 37 °C, then the cells were treated with Yoda1 (5 μM) or GsMTx4. The intracellular
332 calcium ions were measured at room temperature using a laser confocal microscope
333 with an excitation wave length of 494 nm and an emission wave length of 516 nm.
334 The change of fluorescent signal was presented as$\Delta F/F0$ and plotted against time.
335
336 **Whole-cell Patch-Clamp recording**
337 Borosilicate glass-made patch pipettes (BF150-86-7.5, Sutter Instrument Co,
338 USA) were pulled with micropipette puller (P-1000, Sutter Instrument Co, USA) to a
339 resistance of 3–5 MΩ after being filled with pipette solution: 138mM KCl, 10mM
340 NaCl, 1mM $MgCl_2$, 10mM Glucose and 10mM HEPES (pH 7.4). Cells were bathed
341 in Margo-Ringer solution: 130mM NaCl, 5mM KCl, 1mM $MgCl_2$, 2.5mM $CaCl_2$,
342 10mM Glucose, 20mM HEPES (pH7.4). Whole-cell calcium currents of STC-1 cells
343 were recorded with the EPC10 USB patch-clamp amplifier (HEKA, Germany)
344 controlled by PatchMaster software.
345
346 **Key resource**
347 Key reagents or resources are listed in the SI Appendix, Table S3.
348

Statistical Analysis

All data were expressed as mean ± S.E.M. Statistical differences were evaluated by one-way ANOVA or Student's t-test. The correlation was determined by Pearson analysis. $P < 0.05$ was considered significant. (*$p < 0.05$, **$p < 0.01$, *** $p < 0.001$, ns=not significance).

356 **Results**

357 **Assessment of Piezo1 in human and mouse intestine in different energy status**

358 *Piezo1* mRNA was found to be highly expressed in both mouse ileal mucosa and
359 STC-1 cells (Figure supplement 1A). Moreover, Piezo1 was co-localized with GLP-1
360 in immunofluorescent staining on NCD fed mouse ileal sections, indicating its
361 expression in L cells (Figure supplement 1B). Interestingly, increased body weight
362 and impaired glucose tolerance were observed in high-fat diet-induced diabetic mice,
363 while Piezo1 and Proglucagon expression levels in the ileal mucosa of diabetic mice
364 were significantly lower than that in mice feed with normal chow diet (Figure
365 supplement 1C-F). Moreover, ileal mucosal *Piezo1* mRNA levels were positively
366 correlated with *Proglucagon* mRNA levels (Figure supplement 1G), but negatively
367 correlated with the AUC of glucose tolerance test (Figure supplement 1H). Obese
368 T2MD patients who underwent Roux-en-Y gastric bypass (RYGB) surgery showed
369 decreased BMI (Figure supplement 1I) and increased *Piezo1* and GLP-1 in ileal
370 mucosa (Figure supplement 1J and K) compared to that before surgery. These
371 findings indicated that Piezo1 is expressed in intestinal L cells and its level varies in
372 different energy status.

373

374 **Generation and characterization of *IntL-Piezo1*$^{-/-}$ mice**

375 To investigate the potential role of Piezo1 in GLP-1 production, we tried to
376 knockout *Piezo1* in L cells by Cre-loxP system driven by an L cell-specific promoter.
377 Proglucagon (encoded by *Gcg* gene) is mainly expressed in both L cells and
378 pancreatic α cells (Jin, 2008). Villin-1 (encoded by *Vil1* gene) is expressed in
379 gastrointestinal epithelium, including L cells, but not in pancreatic α cells (Maunoury
380 et al., 1992; Rutlin et al., 2020). Since neither Gcg nor Villin are specific markers for
381 L cells, we tried to generate a new line of mice enabling loss of Piezo1 expression
382 specifically in the intestine L cell by combination of Flp-Frt and Cre-loxP system. We
383 inserted a Flippase (Flp) expression cassette in the 3'UTR of *Vil1* to generate a *Vil1*
384 promoter-driven Flp mice (*Vil-Flp*) (Fig. 1A). Then, we generated Flippase-dependent
385 Gcg promoter driven-Cre (*FGC*) mice by inserting an Frt-flanked Cre expression
386 cassette in reverse orientation within the 3'- UTR of *Gcg* gene (Figure 1A). We
387 further crossed the *Vil-Flp* mice with *FGC* mice to obtain L cell specific Cre mice
388 (*IntL-Cre*), in which *Vil1* promoter-driven Flippase flipped the reverse Cre cassette
389 into a correct orientation in Villin positive cells (including L cells, but not pancreatic
390 α cells), and thus Cre can only be expressed under the *Gcg* promoter in L cells. The
391 genotypes of the *Vil-Flp*, *FGC* and *IntL-Cre* mice were identified by PCR with
392 specific primers (Figure 1B). The flipping of the reverse Cre cassette was validated by
393 PCR, which confirmed that the flipping only occurred the intestine, but not in the
394 pancreas (Figure 1C). To confirm the cell type specificity of Cre activity, we crossed
395 *IntL-Cre* mice to *mT/mG* reporter mice. All tissues and cells of *mT/mG* mice express
396 red fluorescence (membrane-targeted tdTomato; mT) at baseline, and switch to
397 membrane-targeted EGFP in the presence of cell-specific Cre (Figure 1D). EGFP
398 expression was only observed scatteredly in the intestine, but not in the pancreas,
399 indicating the L cell-specific Cre activity in the *IntL-Cre* mice (Figure 1E). Finally,
400 we bred *IntL-Cre* mice with *Piezo1*$^{loxp/loxp}$ mice to generate *IntL-Piezo1*$^{-/-}$ mice (Figure
401 1F).

402 Under normal chow diet, *IntL-Piezo1*$^{-/-}$ mice exhibited increased body weight
403 (Figure 1G) and greater glycemic excursions compared to control groups
404 (*Piezo1*$^{loxp/loxp}$, *Vil-Flp*, *FGC* and *IntL-cre*) (Figure 1H and I), while the food and
405 water intake were not changed (Figure 1-figure supplement 2A and B). The
406 morphology of islet (Figure 1-figure supplement 3A) and ileum (Figure 1-figure
407 supplement 4A) were not affected. Ileal mucosal Proglucagon expression and plasma
408 GLP-1 level were significantly lower in *IntL-Piezo1*$^{-/-}$ mice than that in all littermate
409 controls such as *Piezo1*$^{loxp/loxp}$, *Vil-Flp*, *FGC* and *IntL-Cre* mice (Figure 1J and K),
410 while no significant alteration was observed in the expression of pancreatic Piezo1
411 and Proglucagon (Figure 1-figure supplement 3B-D), as well as ileal mucosal
412 cholecystokinin (CCK), another hormone secreted by L cells (Figure 1-figure
413 supplement 5). According to in situ hybridization of Piezo1 and GLP-1, the
414 expression of Piezo1 disappeared in GLP-1 positive cells, suggesting successful
415 knockout of Piezo1 in L cells in *IntL-Piezo1*$^{-/-}$ mice (Figure 1L and M).

416 Piezo1 is a non-selective cationic channel that allows passage of Ca^{2+} and Na^{+}.
417 CaMKKβ is the main calcium/calmodulin dependent protein kinase kinase involved
418 in the regulation of metabolic homeostasis (Marcelo et al., 2016). It is activated by
419 binding calcium-calmodulin (Ca^{2+}/CaM), resulting in downstream activation of
420 kinases CaMKIV. The activation of CaMKIV modulate the gene expression of
421 nutrient- and hormone-related proteins (Ban et al., 2000; Chen et al., 2011;
422 Takemoto-Kimura et al., 2017). Previous studies have reported that Ca^{2+} and mTOR
423 signaling regulate the production of GLP-1 (Tolhurst et al., 2011; Xu et al., 2015; Yu
424 & Jin, 2010). Drawing from these findings, we hypothesized that Piezo1 might
425 regulate GLP-1 synthesis through the CaMKKβ/CaMKIV-mTOR signaling pathway
426 (Figure 1N). As shown in Figure 1O, abrogated GLP-1 production was associated
427 with decreased CaMKKβ/CaMKIV-mTOR signaling in the ileal mucosa of
428 *IntL-Piezo1*$^{-/-}$ mice (Figure 1O).

429 **Derangements of glucose metabolism and glp-1 production were induced by**
430 **HFD in *IntL-Piezo1*$^{-/-}$ mice, which was mitigated by Exendin-4**

431 We next assessed the effect of L cell-specific *Piezo1* gene deletion on GLP-1 and
432 glucose tolerance in diet-induced diabetic mice. *IntL-Piezo1*$^{-/-}$ and control mice were
433 exposed to HFD for 10 weeks. Compared to the controls, higher body weight (Figure
434 2A), greater glucose excursions (Figure 2B) were observed in *IntL-Piezo1*$^{-/-}$ mice
435 exposed to HFD. Ileal mucosal Proglucagon expression levels were lower in
436 *IntL-Piezo1*$^{-/-}$ than control mice (Figure 2C-F). Impaired
437 CaMKKβ/CaMKIV-mTORC1 signaling pathway in ileal mucosa as evidenced by a
438 decrease in CaMKKβ, reduced phosphorylation levels of CaMKIV, mTOR, S6K, and
439 S6 was also observed in *IntL-Piezo1*$^{-/-}$ mice (Figure 2F). No significant alteration in
440 morphology, Piezo1 or Proglucagon levels were observed in the pancreas of
441 *IntL-Piezo1*$^{-/-}$ mice (Figure 2-figure supplement 3E-H). Together these data
442 demonstrate that *IntL-Piezo1*$^{-/-}$ mice with prolonged HFD feeding exhibit impaired
443 glucose metabolism phenotype and reduced GLP-1.

444 Injection of GLP-1 analog Exendin-4 (Ex4) decreased the body weight (Figure
445 2G) and improved both glucose tolerance (Figure 2H) and insulin resistance (Figure
446 2I) in control and *IntL-Piezo1*$^{-/-}$ mice, while endogenous synthesis of GLP-1 was not
447 changed by Ex4 injection in *IntL-Piezo1*$^{-/-}$ mice (Figure 2J and K). These data
448 suggested that decreased GLP-1 synthesis and secretion contribute to impaired
449 glucose metabolism in *IntL-Piezo1*$^{-/-}$ mice.
450

451 **The pharmacological and mechanical activation of ileal Piezo1 stimulates GLP-1**
452 **synthesis**

453 We next examined whether activation of Piezo1 could rescued the impaired
454 glucose metabolism in diet-induced diabetic mice. Injection of Piezo1 activator
455 Yoda1 after 10 weeks of high-fat diet, led to reduced body weight and improved the
456 impaired glucose metabolism significantly in diabetic mice, while Piezo1 antagonist
457 GsMTx4 reversed the weight loss and glucose-lowering effect of Yoda1 (Figure 3A
458 and B). Yoda1 remarkably induced an increase in GLP-1 synthesis and secretion
459 (Figure 3C and D), as well as an increment of CaMKKβ/CaMKIV-mTORC1
460 signaling in ileal mucosa (Figure 3E), while GsMTx4 abolished the effect of Yoda1
461 (Figure 3C-E). However, weight loss, improved plasma glucose and increased GLP-1
462 production induced by Yoda1 were not observed in *IntL-Piezo1*$^{-/-}$ mice (Figure 3F-J).

463 The intestine receives mechanical stimulation from the chyme, which may
464 activate Piezo1 in the intestine epithelium, including L cells. To mimic the
465 mechanical pressing and stretching induced by intestinal contents, a small silicon bead
466 was implanted into the high-fat diet-induced diabetic mouse ileum. Intestinal bead
467 implantation improved the impaired glucose metabolism in diabetic mice (Figure 3K
468 and L). Body weight loss, activated ileal mucosal CaMKKβ/CaMKIV-mTOR
469 signaling, increased mRNA and protein levels of ileal mucosal Piezo1 and
470 Proglucagon, as well as the circulating levels of GLP-1 were observed in diabetic
471 mice after operation (Figure 3M-R). The above data suggest that mechanical stimuli
472 induced by intestinal bead implantation activates ileal Piezo1 in diabetic mice,
473 stimulating GLP-1 production via CaMKKβ/CaMKIV-mTOR signaling axis, thus
474 improving glucose homeostasis.
475

476 **Piezo1 regulates GLP-1 synthesis and secretion in primary cultured mouse L**
477 **cells and isolated mouse ileum.**

478 To obtain primary L cells, we isolated cell from the ileum of *IntL-Cre-mT/mG*
479 mice, in which tdTomato expression switched to EGFP expression in L cells as shown
480 in Figure 1E. EGFP positive cells (mouse L cells) were then sorted from isolated
481 single cells (Figure 4A). Immunofluorescence showed that the sorted EGFP+ cells
482 were Piezo1 positive (Figure 4B).

483 Yoda1 at the dose of 5μM triggered an increase in intracellular Ca^{2+} level in
484 primary cultured mouse L cells, which was blocked by pre-incubation of cells with
485 GsMTx4 (0.1 μM) for 15 min (Figure 4C). Yoda1 also stimulated Proglucagon
486 expression and GLP-1 secretion, as well as CaMKKβ/CaMKIV-mTOR signaling
487 pathway in primary cultured mouse L cells (Figure 4D-F). In contrast, knockdown of
488 Piezo1 by shRNA led to significant decrease in Proglucagon expression and GLP-1
489 secretion, as well as inhibition of CaMKKβ/CaMKIV/mTOR signaling pathway
490 (Figure 4G-J).

491 Given the ability of Piezo1 in sensing mechanical force, tension of 1.5g was
492 applied to the isolated mouse ileum bathed in Tyrode's solution for two hours.
493 Tension stimulated Proglucagon expression, GLP-1 secretion and activated
494 CaMKKβ/CaMKIV-mTOR signaling pathway in the ileum of control mice, but not in
495 *IntL-Piezo1*$^{-/-}$ mice (Figure 4K-N), suggesting the involvement of Piezo1 of the L
496 cells in mediating the force-induced GLP-1 production and
497 CaMKKβ/CaMKIV-mTOR signaling.

498

499 **Pharmacological, mechanical and genetic activation of Piezo1 stimulates GLP-1**
500 **synthesis and secretion in STC-1 cells**

501 To further validate the role of Piezo1 in regulating GLP-1, we examined the
502 effect of manipulating Piezo1 on GLP-1 production in an intestinal neuroendocrine
503 cell line STC-1. Pharmacological activation of Piezo1 by Yoda1 triggered an inward
504 current in STC-1 cell recorded by whole cell patch-clamp, which could be inhibited
505 by pre-incubation of GsMTx4 (Figure 5A). Yoda1 also triggered an increase in
506 intracellular Ca^{2+} level in STC-1 cells. Pre-incubation of cells with GsMTx4 (0.1 μM)
507 for 15 min inhibited $[Ca^{2+}]_i$ increase (Figure 5B and C). Yoda1 induced a
508 concentration-dependent activation of CaMKKβ/CaMKIV-mTOR pathway and
509 GLP-1 synthesis and secretion (Figure 5D-F). GsMTx4 blocked the effect of Yoda1
510 on STC-1 cells in both GLP-1 and CaMKKβ/CaMKIV-mTOR activation (Figure
511 5G-I).

512 To mimic the activation of Piezo1 by mechanical stretching in vivo, STC-1 cells
513 grown on elastic chambers were subjected to mechanical stretch to 120% of their
514 original length. Mechanical stretch upregulated Piezo1 and Proglucagon expression,
515 promoted GLP-1 secretion (Figure 5J-M), and activated CaMKKβ/CaMKIV- mTOR
516 signaling pathways (Figure 5M).

517 Consistent to the pharmacological and mechanical activation of Piezo1,
518 over-expression of Piezo1 in STC-1 cells resulted in a significant increase in GLP-1
519 production, as well as activation of the CaMKKβ/CaMKIV-mTOR signaling pathway
520 (Figure 6A-D). Conversely, knockdown of Piezo1 by shRNA led to a significant
521 decrease in GLP-1 production and inhibition of CaMKKβ/CaMKIV-mTOR signaling
522 pathways (Figure 6E-H).
523

524 **Piezo1 regulates GLP-1 production through CaMKKβ/CaMKIV and mTOR in**
525 **STC-1 cells**

526 Next, we examined whether CaMKKβ/CaMKIV and mTOR signaling mediates
527 the effects of Piezo1 on GLP-1 production. Overexpression of CaMKKβ or CaMKIV
528 increased CaMKKβ/CaMKIV and mTOR signaling activity, resulting in increased
529 synthesis and secretion of GLP-1 (Figure 7A-C). In contrast, the CaMKKβ inhibitor
530 STO-609, downregulated CaMKKβ/CaMKIV and mTOR signaling, as well as GLP-1
531 synthesis and secretion (Figure 7D-F). Inhibition of mTORC1 activity by rapamycin
532 suppressed GLP-1 production induced by Yoda1, which was associated with
533 inhibition of mTOR signalling (Figure 7G-I).
534

535 **Discussion**

536 It has been known for decades that GLP-1 secretion from the intestinal L cells is
537 stimulated by meal intake and is essential for postprandial glycemic control (Drucker,
538 2006; Song et al., 2019). However, the mechanism underlying the regulation of
539 GLP-1 production is not completely understood. One of the problems that impeded
540 the investigation of regulation mechanism of GLP-1 is the lack of an L cell-specific
541 genetically engineered animal model. Here, we generated an L cell-specific Cre
542 mouse line for the first time by combination of the Flp-Frt and Cre-LoxP systems,
543 which allows genetic manipulation specifically in the L cells and thus creates a useful
544 tool to investigate molecular mechanisms in L cells.

545 Previous studies have shown that L cells are able to sense nutrients in the
546 intestinal lumen such as glucose and other carbohydrates, lipids and amino acids,
547 which induce GLP-1 secretion through different mechanisms, including membrane
548 depolarization-associated exocytosis, Ca^{2+}/Calmodulin (Tolhurst et al., 2011), cAMP
549 (Yu & Jin, 2010), mTORC1 (Xu et al., 2015) and AMPK (Jiang et al., 2016) signaling
550 pathways. However, it is innegligible that as open type endocrine cells, L cells not
551 only receive the chemical stimulations from the nutrients, but also mechanical
552 stimulation when the chyme passing through the intestine, including stretching,
553 pressure and shear force (Sensoy, 2021). Here, we showed the expression of the
554 mechano-sensitive ion channel Piezo1 in L cells of human and mouse intestinal
555 sections, mouse primary L cell culture and an intestinal neuroendocrine cell line
556 STC-1, suggesting the mechano-sensing ability of L cells and potential regulation of
557 GLP-1 in response to mechanical stimulation. Indeed, our study showed that the
558 mechano-regulation of GLP-1 secretion did exist as demonstrated by the increased
559 GLP-1 secretion by intestinal bead implantation, intestinal tissue stretching or STC-1
560 cell stretching. Moreover, mice with selective loss of Piezo1 expression in intestinal L
561 cell (*IntL-Piezo1*$^{-/-}$) exhibited reduced circulating levels of GLP-1, increased body
562 weight and impaired glucose homeostasis, while pharmacological activation of Piezo1
563 on mice, primary L cells and STC-1 cells did the reverse. More importantly,

564 *IntL-Piezo1*$^{-/-}$ mice was unable to response to the tension-induced GLP-1 production.
565 These further suggested a Piezo1-mediated mechanical sensing mechanism in L cells
566 that regulates GLP-1 production and glucose metabolism by sensing the stimulation
567 of intestinal luminal contents.

568 Interestingly, this intestinal Piezo1-mediated mechanical sensing mechanism
569 may severely impaired in diabetic patients and rodents. We observed a decreased
570 Piezo1 expression in the ileal mucosa of diet-induced diabetic mice accompanied by
571 reduced GLP-1 production. When challenged with high-fat, *IntL-Piezo1*$^{-/-}$ mice
572 exhibited more severe symptoms of diabetes which was mitigated by Ex-4. These
573 findings suggest that the impairment of Piezo1-midated mechanical sensing function
574 in the intestine is an important mechanism for the pathogenesis of T2DM. It is
575 noteworthy that RYGB, a commonly performed weight-loss and hypoglycemic
576 surgery (Cummings et al., 2004), significantly increased Piezo1 expression in L cells
577 of obese diabetic patients. Yoda1 treatment or intestinal bead implantation enhanced
578 GLP-1 production and improved glucose metabolism in the diet-induced diabetic
579 mouse model, suggesting that restore the mechano-sensing or enhance the function of
580 Piezo1 either pharmacologically or mechanically, may be a new strategy to improve
581 the secretion of GLP-1, thus alleviate T2DM. However, in our study, the
582 Piezo1-mediated regulation of GLP-1 production is only demonstrated in transgenic
583 mice, mouse primary L cells and an intestinal neuroendocrine cell line derived from
584 mouse. Whether Piezo1 plays the same role in human L cells awaits to be investigated.
585 A number of studies have generated L cells culture from human intestinal organoid
586 culture or human intestinal stem cell monolayer culture by manipulating the growth
587 factors in the media (Goldspink et al., 2020; Petersen et al., 2014; Villegas-Novoa et
588 al., 2022). It is worthy to validate our finding in human L cells in order to prove its
589 translational potential in T2DM treatment.

590 The intragastric balloon is a current noninvasive clinical weight loss measure
591 that involves placing a space-occupying balloon in the stomach to reduce food intake
592 and generate satiety signals, thus maintaining satiety. Investigations illustrated that

593 intragastric balloon alter the secretion of hormones such as cholecystokinin and
594 pancreatic polypeptide, delay the emptying of food in the stomach and reduce the
595 appetite (Mathus-Vliegen & de Groot, 2013). Intragastric balloon provides a feasible
596 weight loss intervention for obese people (Kim et al., 2016). In this study, a new
597 intestinal implantation surgery of beads was adopted, which may offer a novel
598 approach for weight loss and glucose control by activating the intestinal
599 Piezo1-GLP-1 signaling pathway in the future.

600 Mechanistically, our study suggest that Piezo1 regulates GLP-1 production
601 through a CaMKKβ/CaMKIV-mTOR signaling pathway. CaMKKβ/CaMKIV has
602 been reported to mediate the Ca^{2+} signaling in many metabolic processes, including
603 liver gluconeogenesis and de novo lipogenesis, adipogenesis, insulin sensitivity and β
604 cell proliferation (Anderson et al., 2012; Lin et al., 2011; Liu et al., 2012; J. Liu et al.,
605 2022). mTOR plays a central role in nutrient and energy sensing and regulates cellular
606 metabolism and growth in response to different nutrient and energy status (Howell &
607 Manning, 2011). Here we showed that mTOR can also response to mechanical stimuli
608 through a mechano-sensitive Ca^{2+} channel mediated CaMKKβ/CaMKIV activation.
609 Although we did not demonstrate direct phosphorylation of mTOR or S6K by
610 CaMKIV in L cells, previous study reported that CaMKK2 could serve as a scaffold
611 to assemble CaMKIV with key components of the mTOR/S6K pathway and promote
612 liver cancer cell growth (Lin et al., 2015), which lend support to the
613 CaMKKβ/CaMKIV-mTOR signaling in our study. Recently, Knutson et. al. found
614 that ryanodine and IP3-triggered calcium release from intracellular calcium store
615 could amplified the initial Peizo2 - Ca^{2+} signal triggered by mechanical stimulation,
616 and was required for the mechanotransduction in the serotonin release from
617 enterochromaffin cells (Knutson et al., 2023). In our study, we also observed
618 long-lasting intracellular Ca^{2+} increase triggered by Yoda1 in primary L cells and
619 STC-1 cells, which also suggested an involvement of intracellular Ca^{2+} store in the
620 Ca^{2+} relay. Beside Ca^{2+}, cyclic AMP (cAMP) is another signaling molecule that active
621 *Gcg* gene expression and GLP-1 production (Drucker et al., 1994; Jin, 2008; Simpson

622 et al., 2007). cAMP was found to play a critical role in nutrients-induced GLP-1
623 secretion, including glucose (Ong et al., 2009), lipids (Hodge et al., 2016), and amino
624 acids (Tolhurst et al., 2011). Previous study reported that Ca^{2+} can activate soluble
625 adenylyl cyclase (sAC) to increase intracellular cAMP (Jaiswal & Conti, 2003).
626 Whether sAC-cAMP can be activated by Piezo1-mediated Ca^{2+} influx and whether it
627 is an alternative signaling pathway that mediates the Piezo1-regulated GLP-1
628 production remain to be explored.

629 In summary, our study reveals a previously undiscovered Piezo1-mediated
630 mechano-sensing property of intestinal L cell, which plays an essential role in the
631 regulation of GLP-1 production and glucose metabolism. This finding also suggests a
632 new mechano-regulation in enteroendocrine cells, in addition to chemical and
633 neuronal regulation, which may shed new light on the strategy for metabolic diseases
634 such as diabetes and obesity.

Acknowledgements

Funding

This work was supported by grants from the National Natural Science Foundation of China (82170818, 81770794), Guangdong Basic and Applied Basic Research Foundation (2024A1515010686), the Fundamental Research Funds for the Central Universities (21620423), Guangzhou Science and Technology Plan Project Funding (202201011353).

Conflicts of interest

On behalf of all authors, the corresponding author states that there is no conflict of interest.

Author contribution

Geyang Xu and Hui Chen designed research; Yanling Huang, Haocong Mo, Jie Yang, Luyang Gao, Tian Tao, Qing Shu, Wenying Guo, Yawen Zhao, Jingya Lyu, Qimeng Wang, Jinghui Guo, Hening Zhai, Linyan Zhu and Hui Chen performed research; Yanling Huang, Haocong Mo, Jie Yang, Hui Chen and Geyang Xu analyzed data; Geyang Xu and Hui Chen wrote and edited the paper. All authors contributed to the discussion and revision of the article and all approved the final versions of the manuscript. Geyang Xu is responsible for the integrity of the work as a whole.

Ethical Statement

Animals used in this study were handled in accordance with the Guide for the Care and Use of Laboratory Animals published by the National Institutes of Health (NIH Publications No. 8023, revised 1978). All animal protocols were approved by the Animal Care and Use Committee of Jinan University.

Human subject research was approved by the Institutional Review Board of Jinan University.

Reference

Alcaino, C., Knutson, K. R., Treichel, A. J., Yildiz, G., Strege, P. R., Linden, D. R., . . . Beyder, A. (2018). A population of gut epithelial enterochromaffin cells is mechanosensitive and requires Piezo2 to convert force into serotonin release. *Proc Natl Acad Sci U S A*, *115*(32), E7632-e7641. https://doi.org/10.1073/pnas.1804938115

Anderson, K. A., Lin, F., Ribar, T. J., Stevens, R. D., Muehlbauer, M. J., Newgard, C. B., & Means, A. R. (2012). Deletion of CaMKK2 from the liver lowers blood glucose and improves whole-body glucose tolerance in the mouse. *Mol Endocrinol*, *26*(2), 281-291. https://doi.org/10.1210/me.2011-1299

Anini, Y., Hansotia, T., & Brubaker, P. L. (2002). Muscarinic receptors control postprandial release of glucagon-like peptide-1: in vivo and in vitro studies in rats. *Endocrinology*, *143*(6), 2420-2426. https://doi.org/10.1210/endo.143.6.8840

Atanga, R., Singh, V., & In, J. G. (2023). Intestinal Enteroendocrine Cells: Present and Future Druggable Targets. *Int J Mol Sci*, *24*(10). https://doi.org/10.3390/ijms24108836

Ban, N., Yamada, Y., Someya, Y., Ihara, Y., Adachi, T., Kubota, A., . . . Seino, Y. (2000). Activating transcription factor-2 is a positive regulator in CaM kinase IV-induced human insulin gene expression. *Diabetes*, *49*(7), 1142-1148. https://doi.org/10.2337/diabetes.49.7.1142

Bany Bakar, R., Reimann, F., & Gribble, F. M. (2023). The intestine as an endocrine organ and the role of gut hormones in metabolic regulation. *Nat Rev Gastroenterol Hepatol*. https://doi.org/10.1038/s41575-023-00830-y

Bezin, J., Gouverneur, A., Pénichon, M., Mathieu, C., Garrel, R., Hillaire-Buys, D., . . . Faillie, J. L. (2023). GLP-1 Receptor Agonists and the Risk of Thyroid Cancer. *Diabetes Care*, *46*(2), 384-390. https://doi.org/10.2337/dc22-1148

Cahalan, S. M., Lukacs, V., Ranade, S. S., Chien, S., Bandell, M., & Patapoutian, A. (2015). Piezo1 links mechanical forces to red blood cell volume. *Elife*, *4*. https://doi.org/10.7554/eLife.07370

Chen, K., Yu, X., Murao, K., Imachi, H., Li, J., Muraoka, T., . . . Tokumitsu, H. (2011). Exendin-4 regulates GLUT2 expression via the CaMKK/CaMKIV pathway in a pancreatic β-cell line. *Metabolism*, *60*(4), 579-585. https://doi.org/10.1016/j.metabol.2010.06.002

Cummings, D. E., Overduin, J., & Foster-Schubert, K. E. (2004). Gastric bypass for obesity: mechanisms of weight loss and diabetes resolution. *J Clin Endocrinol Metab*, *89*(6), 2608-2615. https://doi.org/10.1210/jc.2004-0433

Deivasikamani, V., Dhayalan, S., Abudushalamu, Y., Mughal, R., Visnagri, A., Cuthbertson, K., . . . Sukumar, P. (2019). Piezo1 channel activation mimics high glucose as a stimulator of insulin release. *Sci Rep*, *9*(1), 16876. https://doi.org/10.1038/s41598-019-51518-w

Diakogiannaki, E., Gribble, F. M., & Reimann, F. (2012). Nutrient detection by incretin hormone secreting cells. *Physiol Behav*, *106*(3), 387-393. https://doi.org/10.1016/j.physbeh.2011.12.001

Drucker, D. J. (2006). The biology of incretin hormones. *Cell Metab*, *3*(3), 153-165. https://doi.org/10.1016/j.cmet.2006.01.004

Drucker, D. J., Jin, T., Asa, S. L., Young, T. A., & Brubaker, P. L. (1994). Activation of proglucagon gene transcription by protein kinase-A in a novel mouse enteroendocrine cell line. *Mol Endocrinol*, *8*(12), 1646-1655. https://doi.org/10.1210/mend.8.12.7535893

Elashoff, M., Matveyenko, A. V., Gier, B., Elashoff, R., & Butler, P. C. (2011). Pancreatitis, pancreatic, and thyroid cancer with glucagon-like peptide-1-based therapies. *Gastroenterology*, *141*(1), 150-156. https://doi.org/10.1053/j.gastro.2011.02.018

Furness, J. B., Rivera, L. R., Cho, H. J., Bravo, D. M., & Callaghan, B. (2013). The gut as a sensory organ. *Nat Rev Gastroenterol Hepatol*, *10*(12), 729-740. https://doi.org/10.1038/nrgastro.2013.180

Goldspink, D. A., Lu, V. B., Miedzybrodzka, E. L., Smith, C. A., Foreman, R. E., Billing, L. J., . . . Gribble, F. M. (2020). Labeling and Characterization of Human GLP-1-Secreting L-cells in Primary Ileal Organoid Culture. *Cell Rep*, *31*(13), 107833. https://doi.org/10.1016/j.celrep.2020.107833

Gribble, F. M., & Reimann, F. (2016). Enteroendocrine Cells: Chemosensors in the Intestinal Epithelium. *Annu Rev Physiol*, *78*, 277-299. https://doi.org/10.1146/annurev-physiol-021115-105439

Gudipaty, S. A., Lindblom, J., Loftus, P. D., Redd, M. J., Edes, K., Davey, C. F., . . . Rosenblatt, J. (2017). Mechanical stretch triggers rapid epithelial cell division through Piezo1. *Nature*, *543*(7643), 118-121. https://doi.org/10.1038/nature21407

Hodge, D., Glass, L. L., Diakogiannaki, E., Pais, R., Lenaghan, C., Smith, D. M., . . . Reimann, F. (2016). Lipid derivatives activate GPR119 and trigger GLP-1 secretion in primary murine L-cells. *Peptides*, *77*, 16-20. https://doi.org/10.1016/j.peptides.2015.06.012

733 Howell, J. J., & Manning, B. D. (2011). mTOR couples cellular nutrient sensing to
734 organismal metabolic homeostasis. *Trends Endocrinol Metab*, *22*(3), 94-102.
735 https://doi.org/10.1016/j.tem.2010.12.003

736 Jaiswal, B. S., & Conti, M. (2003). Calcium regulation of the soluble adenylyl cyclase
737 expressed in mammalian spermatozoa. *Proc Natl Acad Sci U S A*, *100*(19),
738 10676-10681. https://doi.org/10.1073/pnas.1831008100

739 Jiang, S., Zhai, H., Li, D., Huang, J., Zhang, H., Li, Z., . . . Xu, G. (2016).
740 AMPK-dependent regulation of GLP1 expression in L-like cells. *J Mol Endocrinol*,
741 *57*(3), 151-160. https://doi.org/10.1530/jme-16-0099

742 Jiang, Y., Song, J., Xu, Y., Liu, C., Qian, W., Bai, T., & Hou, X. (2021). Piezo1
743 regulates intestinal epithelial function by affecting the tight junction protein claudin-1
744 via the ROCK pathway. *Life Sci*, *275*, 119254.
745 https://doi.org/10.1016/j.lfs.2021.119254

746 Jin, T. (2008). Mechanisms underlying proglucagon gene expression. *J Endocrinol*,
747 *198*(1), 17-28. https://doi.org/10.1677/joe-08-0085

748 Kim, S. H., Chun, H. J., Choi, H. S., Kim, E. S., Keum, B., & Jeen, Y. T. (2016).
749 Current status of intragastric balloon for obesity treatment. *World J Gastroenterol*,
750 *22*(24), 5495-5504. https://doi.org/10.3748/wjg.v22.i24.5495

751 Knutson, K. R., Whiteman, S. T., Alcaino, C., Mercado-Perez, A., Finholm, I., Serlin,
752 H. K., . . . Beyder, A. (2023). Intestinal enteroendocrine cells rely on ryanodine and
753 IP(3) calcium store receptors for mechanotransduction. *J Physiol*, *601*(2), 287-305.
754 https://doi.org/10.1113/jp283383

755 Lai, A., Cox, C. D., Chandra Sekar, N., Thurgood, P., Jaworowski, A., Peter, K., &
756 Baratchi, S. (2022). Mechanosensing by Piezo1 and its implications for physiology
757 and various pathologies. *Biol Rev Camb Philos Soc*, *97*(2), 604-614.
758 https://doi.org/10.1111/brv.12814

759 Li, J., Hou, B., Tumova, S., Muraki, K., Bruns, A., Ludlow, M. J., . . . Beech, D. J.
760 (2014). Piezo1 integration of vascular architecture with physiological force. *Nature*,
761 *515*(7526), 279-282. https://doi.org/10.1038/nature13701

762 Li, Z., Bowers, E., Zhu, J., Yu, H., Hardij, J., Bagchi, D. P., . . . MacDougald, O. A.
763 (2022). Lipolysis of bone marrow adipocytes is required to fuel bone and the marrow
764 niche during energy deficits. *Elife*, *11*. https://doi.org/10.7554/eLife.78496

765 Lin, F., Marcelo, K. L., Rajapakshe, K., Coarfa, C., Dean, A., Wilganowski, N., . . .
766 York, B. (2015). The camKK2/camKIV relay is an essential regulator of hepatic
767 cancer. *Hepatology*, *62*(2), 505-520. https://doi.org/10.1002/hep.27832

768 Lin, F., Ribar, T. J., & Means, A. R. (2011). The Ca2+/calmodulin-dependent protein
769 kinase kinase, CaMKK2, inhibits preadipocyte differentiation. *Endocrinology*,
770 *152*(10), 3668-3679. https://doi.org/10.1210/en.2011-1107

771 Liu, B., Barbosa-Sampaio, H., Jones, P. M., Persaud, S. J., & Muller, D. S. (2012).
772 The CaMK4/CREB/IRS-2 cascade stimulates proliferation and inhibits apoptosis of
773 β-cells. *PLoS One*, *7*(9), e45711. https://doi.org/10.1371/journal.pone.0045711

774 Liu, H., Hu, J., Zheng, Q., Feng, X., Zhan, F., Wang, X., . . . Hua, F. (2022). Piezo1
775 Channels as Force Sensors in Mechanical Force-Related Chronic Inflammation. *Front*
776 *Immunol*, *13*, 816149. https://doi.org/10.3389/fimmu.2022.816149

777 Liu, J., Li, Y., Gao, N., Ji, J., & He, Q. (2022). Calcium/calmodulin-dependent protein
778 kinase IV regulates vascular autophagy and insulin signaling through
779 Akt/mTOR/CREB pathway in ob/ob mice. *J Physiol Biochem*, *78*(1), 199-211.
780 https://doi.org/10.1007/s13105-021-00853-6

781 Marcelo, K. L., Means, A. R., & York, B. (2016). The Ca(2+)/Calmodulin/CaMKK2
782 Axis: Nature's Metabolic CaMshaft. *Trends Endocrinol Metab*, *27*(10), 706-718.
783 https://doi.org/10.1016/j.tem.2016.06.001

784 Mathus-Vliegen, E. M., & de Groot, G. H. (2013). Fasting and meal-induced CCK
785 and PP secretion following intragastric balloon treatment for obesity. *Obes Surg*, *23*(5),
786 622-633. https://doi.org/10.1007/s11695-012-0834-6

787 Maunoury, R., Robine, S., Pringault, E., Léonard, N., Gaillard, J. A., & Louvard, D.
788 (1992). Developmental regulation of villin gene expression in the epithelial cell
789 lineages of mouse digestive and urogenital tracts. *Development*, *115*(3), 717-728.
790 https://doi.org/10.1242/dev.115.3.717

791 Ong, W. K., Gribble, F. M., Reimann, F., Lynch, M. J., Houslay, M. D., Baillie, G.
792 S., . . . Pyne, N. J. (2009). The role of the PDE4D cAMP phosphodiesterase in the
793 regulation of glucagon-like peptide-1 release. *Br J Pharmacol*, *157*(4), 633-644.
794 https://doi.org/10.1111/j.1476-5381.2009.00194.x

795 Petersen, N., Reimann, F., Bartfeld, S., Farin, H. F., Ringnalda, F. C., Vries, R. G., . . .
796 de Koning, E. J. (2014). Generation of L cells in mouse and human small intestine
797 organoids. *Diabetes*, *63*(2), 410-420. https://doi.org/10.2337/db13-0991

798 Romac, J. M., Shahid, R. A., Swain, S. M., Vigna, S. R., & Liddle, R. A. (2018).
799 Piezo1 is a mechanically activated ion channel and mediates pressure induced
800 pancreatitis. *Nat Commun*, *9*(1), 1715. https://doi.org/10.1038/s41467-018-04194-9

801 Rouillé, Y., Kantengwa, S., Irminger, J. C., & Halban, P. A. (1997). Role of the
802 prohormone convertase PC3 in the processing of proglucagon to glucagon-like

803 peptide 1. *J Biol Chem*, *272*(52), 32810-32816.
804 https://doi.org/10.1074/jbc.272.52.32810

805 Rutlin, M., Rastelli, D., Kuo, W. T., Estep, J. A., Louis, A., Riccomagno, M. M., . . .
806 Rao, M. (2020). The Villin1 Gene Promoter Drives Cre Recombinase Expression in
807 Extraintestinal Tissues. *Cell Mol Gastroenterol Hepatol*, *10*(4), 864-867.e865.
808 https://doi.org/10.1016/j.jcmgh.2020.05.009

809 Saxena, A. R., Gorman, D. N., Esquejo, R. M., Bergman, A., Chidsey, K., Buckeridge,
810 C., . . . Kim, A. M. (2021). Danuglipron (PF-06882961) in type 2 diabetes: a
811 randomized, placebo-controlled, multiple ascending-dose phase 1 trial. *Nat Med*,
812 *27*(6), 1079-1087. https://doi.org/10.1038/s41591-021-01391-w

813 Sensoy, I. (2021). A review on the food digestion in the digestive tract and the used in
814 vitro models. *Curr Res Food Sci*, *4*, 308-319.
815 https://doi.org/10.1016/j.crfs.2021.04.004

816 Simpson, A. K., Ward, P. S., Wong, K. Y., Collord, G. J., Habib, A. M., Reimann, F.,
817 & Gribble, F. M. (2007). Cyclic AMP triggers glucagon-like peptide-1 secretion from
818 the GLUTag enteroendocrine cell line. *Diabetologia*, *50*(10), 2181-2189.
819 https://doi.org/10.1007/s00125-007-0750-9

820 Song, Y., Koehler, J. A., Baggio, L. L., Powers, A. C., Sandoval, D. A., & Drucker, D.
821 J. (2019). Gut-Proglucagon-Derived Peptides Are Essential for Regulating Glucose
822 Homeostasis in Mice. *Cell Metab*, *30*(5), 976-986.e973.
823 https://doi.org/10.1016/j.cmet.2019.08.009

824 Takemoto-Kimura, S., Suzuki, K., Horigane, S. I., Kamijo, S., Inoue, M., Sakamoto,
825 M., . . . Bito, H. (2017). Calmodulin kinases: essential regulators in health and disease.
826 *J Neurochem*, *141*(6), 808-818. https://doi.org/10.1111/jnc.14020

827 Tan, Q., Akindehin, S. E., Orsso, C. E., Waldner, R. C., DiMarchi, R. D., Müller, T. D.,
828 & Haqq, A. M. (2022). Recent Advances in Incretin-Based Pharmacotherapies for the
829 Treatment of Obesity and Diabetes. *Front Endocrinol (Lausanne)*, *13*, 838410.
830 https://doi.org/10.3389/fendo.2022.838410

831 Tolhurst, G., Zheng, Y., Parker, H. E., Habib, A. M., Reimann, F., & Gribble, F. M.
832 (2011). Glutamine triggers and potentiates glucagon-like peptide-1 secretion by
833 raising cytosolic Ca2+ and cAMP. *Endocrinology*, *152*(2), 405-413.
834 https://doi.org/10.1210/en.2010-0956

835 Treichel, A. J., Finholm, I., Knutson, K. R., Alcaino, C., Whiteman, S. T., Brown, M.
836 R., . . . Beyder, A. (2022). Specialized Mechanosensory Epithelial Cells in Mouse Gut
837 Intrinsic Tactile Sensitivity. *Gastroenterology*, *162*(2), 535-547.e513.
838 https://doi.org/10.1053/j.gastro.2021.10.026

Villegas-Novoa, C., Wang, Y., Sims, C. E., & Allbritton, N. L. (2022). Development of a Primary Human Intestinal Epithelium Enriched in L-Cells for Assay of GLP-1 Secretion. *Anal Chem*, *94*(27), 9648-9655. https://doi.org/10.1021/acs.analchem.2c00912

Wang, J., Sun, Y. X., & Li, J. (2023). The role of mechanosensor Piezo1 in bone homeostasis and mechanobiology. *Dev Biol*, *493*, 80-88. https://doi.org/10.1016/j.ydbio.2022.11.002

Wang, S., Chennupati, R., Kaur, H., Iring, A., Wettschureck, N., & Offermanns, S. (2016). Endothelial cation channel PIEZO1 controls blood pressure by mediating flow-induced ATP release. *J Clin Invest*, *126*(12), 4527-4536. https://doi.org/10.1172/jci87343

Willms, B., Werner, J., Holst, J. J., Orskov, C., Creutzfeldt, W., & Nauck, M. A. (1996). Gastric emptying, glucose responses, and insulin secretion after a liquid test meal: effects of exogenous glucagon-like peptide-1 (GLP-1)-(7-36) amide in type 2 (noninsulin-dependent) diabetic patients. *J Clin Endocrinol Metab*, *81*(1), 327-332. https://doi.org/10.1210/jcem.81.1.8550773

Xu, G., Li, Z., Ding, L., Tang, H., Guo, S., Liang, H., . . . Zhang, W. (2015). Intestinal mTOR regulates GLP-1 production in mouse L cells. *Diabetologia*, *58*(8), 1887-1897. https://doi.org/10.1007/s00125-015-3632-6

Xu, Y., Bai, T., Xiong, Y., Liu, C., Liu, Y., Hou, X., & Song, J. (2021). Mechanical stimulation activates Piezo1 to promote mucin2 expression in goblet cells. *J Gastroenterol Hepatol*, *36*(11), 3127-3139. https://doi.org/10.1111/jgh.15596

Ye, Y., Barghouth, M., Dou, H., Luan, C., Wang, Y., Karagiannopoulos, A., . . . Renström, E. (2022). A critical role of the mechanosensor PIEZO1 in glucose-induced insulin secretion in pancreatic β-cells. *Nat Commun*, *13*(1), 4237. https://doi.org/10.1038/s41467-022-31103-y

Yu, Z., & Jin, T. (2010). New insights into the role of cAMP in the production and function of the incretin hormone glucagon-like peptide-1 (GLP-1). *Cell Signal*, *22*(1), 1-8. https://doi.org/10.1016/j.cellsig.2009.09.032

Zhai, H., Li, Z., Peng, M., Huang, Z., Qin, T., Chen, L., . . . Xu, G. (2018). Takeda G Protein-Coupled Receptor 5-Mechanistic Target of Rapamycin Complex 1 Signaling Contributes to the Increment of Glucagon-Like Peptide-1 Production after Roux-en-Y Gastric Bypass. *EBioMedicine*, *32*, 201-214. https://doi.org/10.1016/j.ebiom.2018.05.026

875 **Figure legends**

876 **Figure 1: Generation, Validation and Characterization of *IntL-Piezo1*$^{-/-}$ mice**

877 (**A**) Schematic description for the generation of Villin-Flippase (*Vil-Flp*) and
878 Flippase-dependent Gcg-Cre (*FGC*) mice. Vil-Flp flip the inverted Cre gene in the
879 Gcg-Cre cassette in *IntL-Cre* mice to restrict Cre expression in intestinal L cells. As
880 shown, Locations of genotyping primers are also indicated.

881 (**B**) Tail DNA genotyping PCR results using genotyping primer for *Vil-Flp*, *FGC* and
882 Flippase-activated Cre (*IntL-Cre*) mice.

883 (**C**) Intestine and pancreas DNA genotyping results. The "Original" band represents
884 the original FGC cassette with inverted Cre, while the "Flipped" band represents
885 recombined FGC cassette with Cre flipped into the correct direction.

886 (**D**) Schematic description for the validation of *IntL-Cre* efficacy by crossing with
887 *mT/mG* reporter mice.

888 (**E**) Fluorescence was detected in the ileal and pancreatic tissues from *mT/mG* and
889 *IntL-Cre-mT/mG* mice by frozen tissue confocal microscopy. Green fluorescence
890 represents successful deletion of TdTomato and reactivation of EGFP in the
891 Cre-expressing cells.

892 (**F**) Schematic description for the generation of Intestinal L cell-Piezo1$^{-/-}$ mice
893 (*IntL-Piezo1*$^{-/-}$) by crossing *Piezo1*$^{loxp/loxp}$ mice with *IntL-Cre* mice.

894 (**G**) Body weight of 14- to 16-week-old male mice of the indicated genotypes fed
895 NCD (n=6/group).

896 (**H-I**) IPGTT (**H**) and ITT (**I**) and associated area under the curve (AUC) values of
897 14- to 16-week-old male mice of the indicated genotypes fed NCD (n=6/group).

898 (**J**) *Proglucagon* mRNA levels in ileum of 14- to 16-week-old male mice of the
899 indicated genotypes fed NCD. (n=6/group).

900 (**K**) The plasma GLP-1 levels in 14- to 16-week-old male mice of the indicated
901 genotypes fed NCD (n=6/group).

902 (**L**) Representative images for Piezo1 RNA-FISH and GLP-1 immunofluorescent
903 staining in the ileum of 14-week-old male mice of indicated genotypes fed NCD
904 (n=6/group).

905 (**M**) Quantitative analysis of Piezo1-positive GLP-1 cells in the ileal mucosa of
906 14-week-old male mice of indicated genotypes fed NCD (n=6/group).

907 (**N**) A schematic diagram depicting the potential mechanisms linking the
908 CaMKKβ/CaMKIV-mTOR signaling pathway and GLP-1 production.

909 (**O**) Representative western blots are shown for indicated antibodies in the ileal
910 mucosa (n = 6/group).

911 Data are represented as mean ± SEM. Significance was determined by Student's t test
912 for comparison between two groups, and by one-way ANOVA for comparison among
913 three groups or more, *$p < 0.05$, **$p < 0.01$, ***$p < 0.001$.

914 **Figure 2: Validation and phenotype of *IntL-Piezo1*$^{-/-}$ mice fed with high-fat diet**
915 (**A**) Body weight of 14- to 16-week-old male *Piezo1*$^{loxp/loxp}$ and *IntL-Piezo1*$^{-/-}$ mice fed
916 with HFD for 10 weeks (n=6/group).
917 (**B**) IPGTT and associated area under the curve (AUC) values of 14- to 16-week-old
918 male *Piezo1*$^{loxp/loxp}$ and *IntL-Piezo1*$^{-/-}$ mice fed with HFD (n=6/group).
919 (**C**) *Proglucagon* mRNA levels in the ileal mucosa of 14- to 16-week-old male
920 *Piezo1*$^{loxp/loxp}$ and *IntL-Piezo1*$^{-/-}$ mice fed with HFD (n=6/group).
921 (**D**) The plasma GLP-1 level in 14- to 16-week-old male *Piezo1*$^{loxp/loxp}$ and
922 *IntL-Piezo1*$^{-/-}$ mice fed with HFD (n=6/group).
923 (**E**) Double immunofluorescent staining of Piezo1, and GLP-1 in the ilea of 14- to
924 16-week-old male *Piezo1*$^{loxp/loxp}$ and *IntL-Piezo1*$^{-/-}$ mice fed HFD (n=6/group).
925 (**F**) Representative western blots are shown for indicated antibodies in the ileal
926 mucosa (n=6/group).
927 (**G**) Body weight after 7 consecutive days infusion of saline or Ex4 (100ug/kg body
928 weight) in 14- to 16-week-old male *Piezo1*$^{loxp/loxp}$ and *IntL-Piezo1*$^{-/-}$ mice fed with
929 HFD (n=6/group).
930 (**H-I**) IPGTT (**H**) and ITT (**I**) and associated area under the curve (AUC) values after
931 consecutive infusion of saline or Ex4.
932 (**J**) *Proglucagon* mRNA levels in the ileal mucosa (n=6/group) after consecutive
933 infusion of saline or Ex4.
934 (**K**) The plasma GLP-1 level after consecutive infusion of saline or Ex4 (n=6/group).
935 Data are represented as mean ± SEM. Significance was determined by Student's t test
936 for comparison between two groups, and by one-way ANOVA for comparison among
937 three groups or more, *$p < 0.05$, **$p < 0.01$, ***$p < 0.001$.
938

Figure 3: Chemical and mechanical interventions of Piezo1 regulates GLP-1 synthesis in mice

(**A**-**E**) 14- to 16-week-old male C57BL/6J mice fed with HFD for 10 weeks were infused with vehicle, Yoda1 (2 μg per mouse) or GsMTx4 (250 μg/kg) by i.p. for 7 consecutive days. (n=6/group).

(**A**) Body weight change after consecutive drug infusion.

(**B**) IPGTT and associated area under the curve (AUC) values.

(**C**) *Proglucagon* mRNA levels in the ileal mucosa.

(**D**) The plasma GLP-1 level.

(**E**) Representative western blots are shown for indicated antibodies in the ileal mucosa.

(**F**-**J**) 14- to 16-week-old male *IntL-Piezo1*$^{-/-}$ mice fed with HFD for 10 weeks were infused with vehicle, Yoda1 (2 μg per mouse) by i.p. for 7 consecutive days. (n=4 or 5/group)

(**F**) Body weight change after 7 consecutive days' drug infusion.

(**G**) Fasting blood glucose levels.

(**H**) Ileal mucosal *Proglucagon* mRNA levels.

(**I**) Plasma GLP-1 levels.

(**J**) Ileal mucosal Proglucagon protein levels.

(**K**-**R**) 14- to 16-week-old male C57BL/6J mice fed with HFD were subjected to sham operation, or intestinal bead implantation (n=6/group).

(**K**) Fasting blood glucose levels.

(**L**) IPGTT and associated area under the curve (AUC) values.

(**M**) Body weight.

(**N** and **O**) *Piezo1* (**N**) and *Proglucagon* (**O**) mRNA levels in the ileal mucosa.

(**P**) The plasma GLP-1 levels.

(**Q**) Immunofluorescence staining of GLP-1 in ileum and quantification of GLP-1 postive cells.

(**R**) Representative western blots images and densitometry quantification for indicated antibodies in the ileal mucosa.

Data are represented as mean ± SEM. Significance was determined by Student's t test for comparison between two groups, and by one-way ANOVA for comparison among three groups or more, *$p < 0.05$, **$p < 0.01$, ***$p < 0.001$.

Figure 4: Piezo1 regulates GLP-1 synthesis and secretion in primary cultured mouse L cells and isolated mouse ileum.

(**A**) Isolation of mouse L cells (GFP positive) from ileal tissue by FACS. The gating in flowcytometry for sorting of GFP positive cells.

(**B**) Immunofluorescent staining of Piezo1 in sorted GFP positive L cells.

(**C**) Intracellular Ca^{2+} imaging by fluo-4-AM calcium probe. The change of fluorescent intensity (ΔF/F0) was plotted against time.

(**D-F**) L cells were treated with vehicle or Yoda1 (5μM) for 24 hours.

(**D**) *Proglucagon* mRNA expression.

(**E**) GLP-1 concentrations in the culture medium.

(**F**) Western blot images and densitometry quantification for the indicated antibodies.

(**G-J**) Knockdown of Piezo1 in L cells by shRNA for 48 hours.

(**G**) *Piezo1* mRNA expression.

(**H**) *Proglucagon* mRNA expression.

(**I**) GLP-1 levels in the culture medium.

(**J**) Western blot images and densitometry quantification for the indicated antibodies.

(**K-N**) Ileal tissues from *Piezo1*$^{loxp/loxp}$ and *IntL-Piezo1*$^{-/-}$ mice were subjected to tension force (n=6/group).

(**K**) A representative photograph showing the traction of isolated ileum.

(**L**) *Proglucagon* mRNA levels.

(**M**) GLP-1 concentrations in the medium.

(**N**) Western blot images and densitometry quantification for the indicated antibodies.

Data are represented as mean ± SEM. n=6. Significance was determined by Student's t test for comparison between two groups, and by one-way ANOVA for comparison among three groups or more, *$p < 0.05$, **$p < 0.01$, ***$p < 0.001$.

Figure 5: Modulation of GLP-1 synthesis and secretion by pharmacological and mechanical activation of Piezo1 in STC-1 cells

(**A**) Whole-cell currents induced by Yoda1 (5μM) were recorded from STC-1 cells or STC-1 cells pretreated with GsMTx4 for 30 min.

(**B** and **C**) Intracellular calcium imaging in STC-1 cells. (**B**) STC-1 cells were loaded with fluo-4 AM for 1 h. The representative time-lapse image showing the intracellular Ca^{2+} signals. (**C**) The change of fluorescent intensity (ΔF/F0) was plotted against time.

(**D-F**) STC-1 cells were treated with various concentrations of Yoda1 for 24 h. (**D**) Whole-cell extracts underwent western blot with indicated antibodies. (**E**) *Proglucagon* mRNA levels. (**F**) GLP-1 concentrations in the culture medium.

(**G-I**) STC-1 cells were treated with Yoda1 (5 μM) in the presence or absence of GsMTx4 (0.1 μM) for 24 h. (**G**) Whole-cell extracts underwent western blot with indicated antibodies. (**H**) *Proglucagon* mRNA levels. (**I**) GLP-1 concentrations in the culture medium.

(**J-M**) STC-1 were subjected to mechanical stretch. (**J**) STC-1 cells were cultured in elastic chambers and the chambers were subjected to mechanical stretch by 120% extension of their original length. The medium GLP-1 concentrations were detected at indicated time. (**K**) *Piezo1* mRNA levels. (**L**) *Proglucagon* mRNA levels (**M**) Whole-cell extracts underwent western blot with indicated antibodies.

Data are represented as mean ± SEM. n=6. Significance was determined by Student's t test for comparison between two groups, and by one-way ANOVA for comparison among three groups or more, *$p < 0.05$, **$p < 0.01$, ***$p < 0.001$.

1023 **Figure 6: Genetic interference of Piezo1 regulates GLP-1 production in STC-1**
1024 **cells**
1025 (**A-D**) STC-1 cells were transfected with mouse control or *Piezo1* expression
1026 plasmids for 48h. *Piezo1* (**A**) and *Proglucagon* (**B**) mRNA levels in STC-1 cells. (**C**)
1027 GLP-1 concentrations in culture medium. (**D**) Whole-cell extracts underwent western
1028 blot with indicated antibodies.
1029 (**E-H**) Stable knockdown of Piezo1 in STC-1 cells. *Piezo1* (**E**) and *Proglucagon* (**F**)
1030 mRNA levels in STC-1 cells. (**G**) GLP-1 concentrations in culture medium. (**H**)
1031 Whole-cell extracts underwent western blot with indicated antibodies.
1032 Data are represented as mean ± SEM. n=6. Significance was determined by Student's
1033 t test, *$p < 0.05$, **$p < 0.01$, ***$p < 0.001$.
1034

1035 **Figure 7: Modulation of GLP-1 production by CaMKKβ/CaMKIV and mTOR**
1036 **signaling activity in STC-1 cells**
1037 (**A-C**) STC-1 cells were transfected with GFP, CaMKKβ or CaMKIV plasmids for
1038 48h. (**A**) *Proglucagon* mRNA levels in STC-1 cells. (**B**) GLP-1 concentrations in
1039 culture medium. (**C**) Whole-cell extracts underwent western blot with indicated
1040 antibodies.
1041 (**D-F**) STC-1 cells were treated with CaMKKβ inhibitor STO-609 (10 μmol/L) for 24
1042 h. (**D**) *Proglucagon* mRNA levels in STC-1 cells. (**E**) GLP-1 concentrations in culture
1043 medium. (**F**) Whole-cell extracts underwent western blot with indicated antibodies.
1044 (**G-I**) STC-1 cells were pretreated with Rapamycin (50 nmol/L) for 1 h, then treated
1045 with Yoda1 (5 μmol/L) for 24 h. (**G**) *Proglucagon* mRNA levels in STC-1 cells. (**H**)
1046 GLP-1 concentrations in the culture medium. (**I**) Whole-cell extracts underwent
1047 western blot with indicated antibodies.
1048 Data are represented as mean ± SEM. n=6. Significance was determined by Student's
1049 t test for comparison between two groups, and by one-way ANOVA for comparison
1050 among three groups or more, *$p < 0.05$, **$p < 0.01$, ***$p < 0.001$.

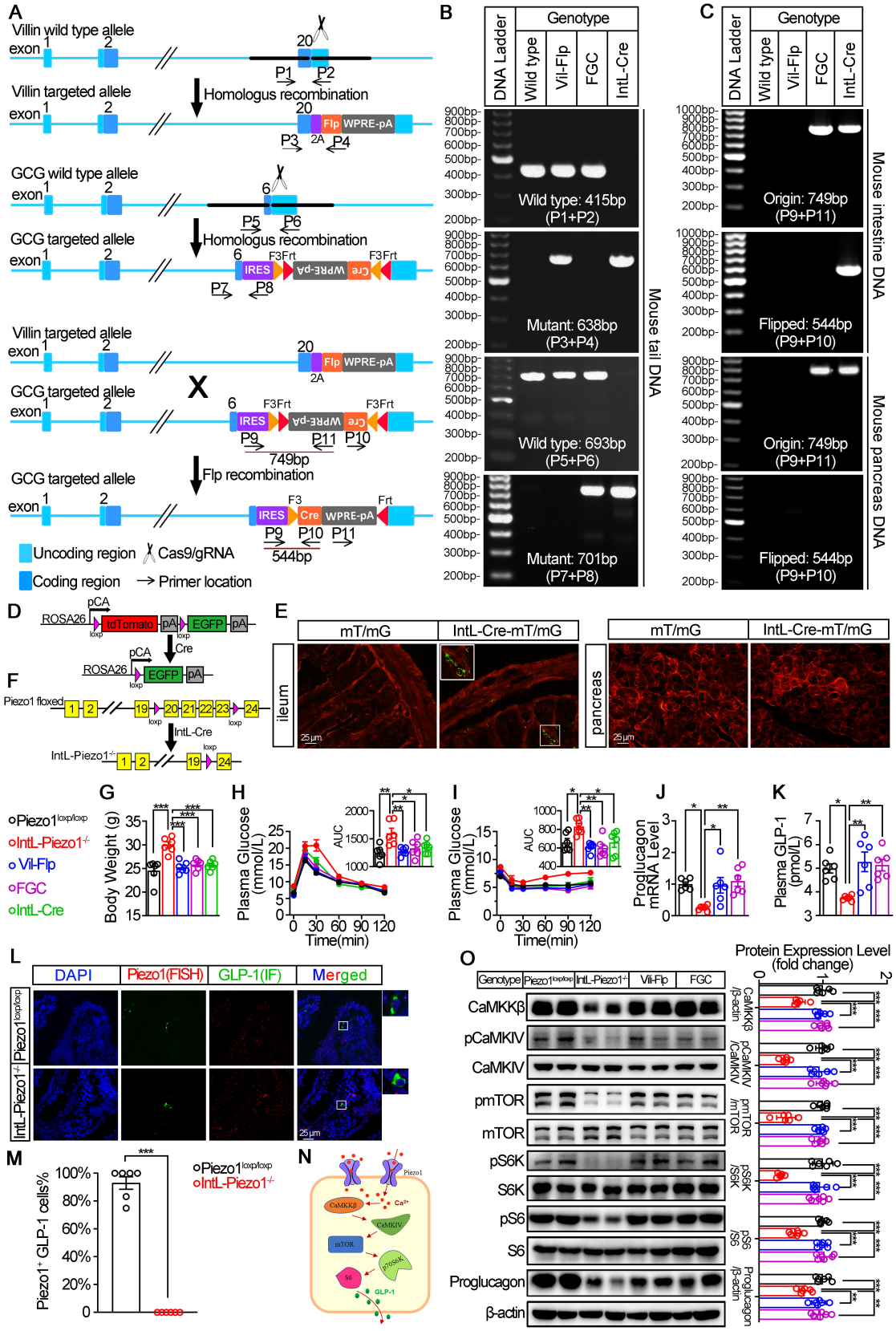
A
Villin wild type allele
exon
Villin targeted allele
Homologus recombination
Flp
WPRE-pA
GCG wild type allele
GCG targeted allele
IRES
F3Frt
Cre
Villin targeted allele
GCG targeted allele
749bp
GCG targeted allele
Flp recombination
544bp
Uncoding region
Cas9/gRNA
Coding region
Primer location
B
DNA Ladder
Genotype
Wild type
Vil-Flp
FGC
IntL-Cre
Wild type: 415bp (P1+P2)
Mutant: 638bp (P3+P4)
Wild type: 693bp (P5+P6)
Mutant: 701bp (P7+P8)
Mouse tail DNA
C
Origin: 749bp (P9+P11)
Flipped: 544bp (P9+P10)
Mouse intestine DNA
Mouse pancreas DNA
D
ROSA26
tdTomato
EGFP
pCA
Cre
F
Piezo1 floxed
IntL-Cre
IntL-Piezo1-/-
E
mT/mG
IntL-Cre-mT/mG
ileum
pancreas
G
Piezo1loxp/loxp
IntL-Piezo1-/-
Vil-Flp
FGC
IntL-Cre
Body Weight (g)
H
Plasma Glucose (mmol/L)
Time(min)
AUC
I
J
Proglucagon mRNA Level
K
Plasma GLP-1 (pmol/L)
L
DAPI
Piezo1(FISH)
GLP-1(IF)
Merged
M
Piezo1+ GLP-1 cells%
N
Piezo1
CaMKKβ
Ca2+
CaMKIV
mTOR
pmTOR/S6K
S6
GLP-1
O
Protein Expression Level (fold change)
CaMKKβ
pCaMKIV
CaMKIV
pmTOR
mTOR
pS6K
S6K
pS6
S6
Proglucagon
β-actin

Figure 1

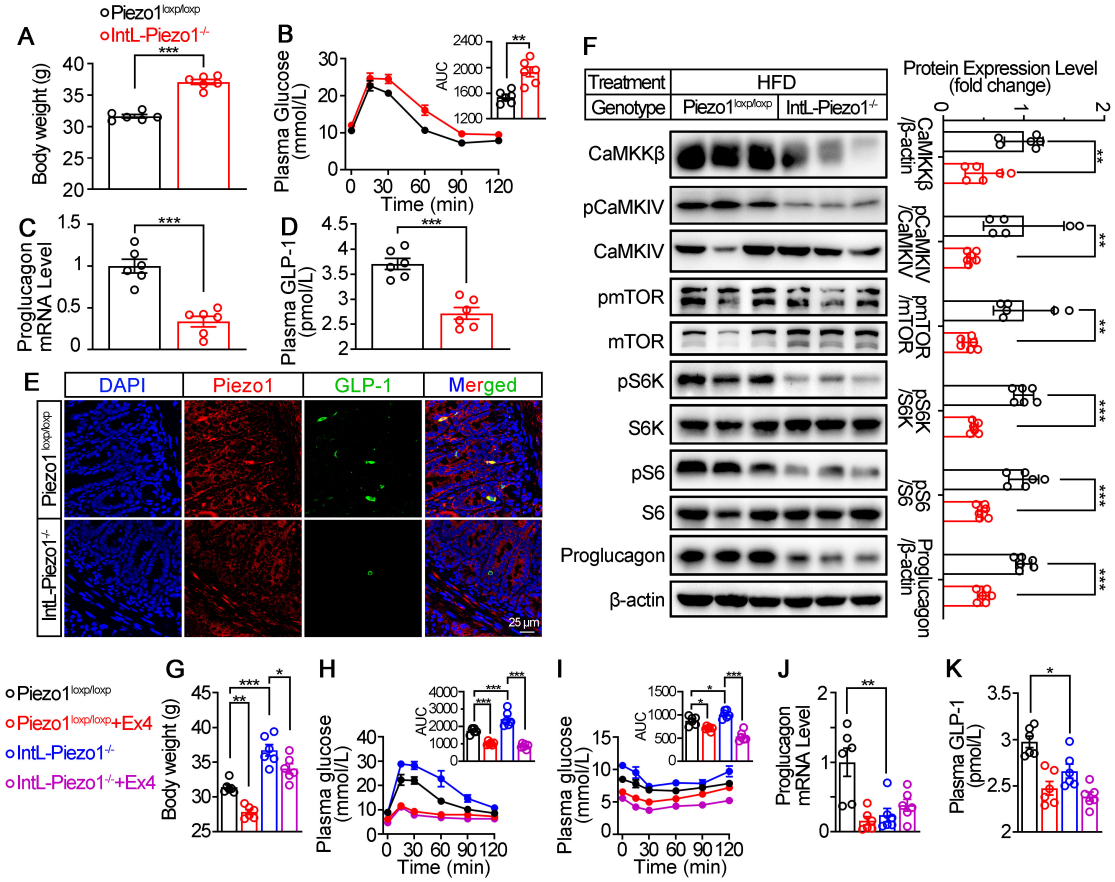
Piezo1loxp/loxp
IntL-Piezo1-/-
A
Body weight (g)
B
Plasma Glucose (mmol/L)
Time (min)
AUC
C
Proglucagon mRNA Level
D
Plasma GLP-1 (pmol/L)
E
DAPI
Piezo1
GLP-1
Merged
25 μm
F
Treatment
HFD
Genotype
Piezo1loxp/loxp
IntL-Piezo1-/-
CaMKKβ
pCaMKIV
CaMKIV
pmTOR
mTOR
pS6K
S6K
pS6
S6
Proglucagon
β-actin
Protein Expression Level (fold change)
CaMKKβ /β-actin
pCaMKIV /CaMKIV
pmTOR /mTOR
pS6K /S6K
pS6 /S6
Proglucagon /β-actin

Piezo1loxp/loxp
Piezo1loxp/loxp+Ex4
IntL-Piezo1-/-
IntL-Piezo1-/-+Ex4
G
Body weight (g)
H
Plasma glucose (mmol/L)
Time (min)
AUC
I
Plasma glucose (mmol/L)
Time (min)
AUC
J
Proglucagon mRNA Level
K
Plasma GLP-1 (pmol/L)

Figure 2

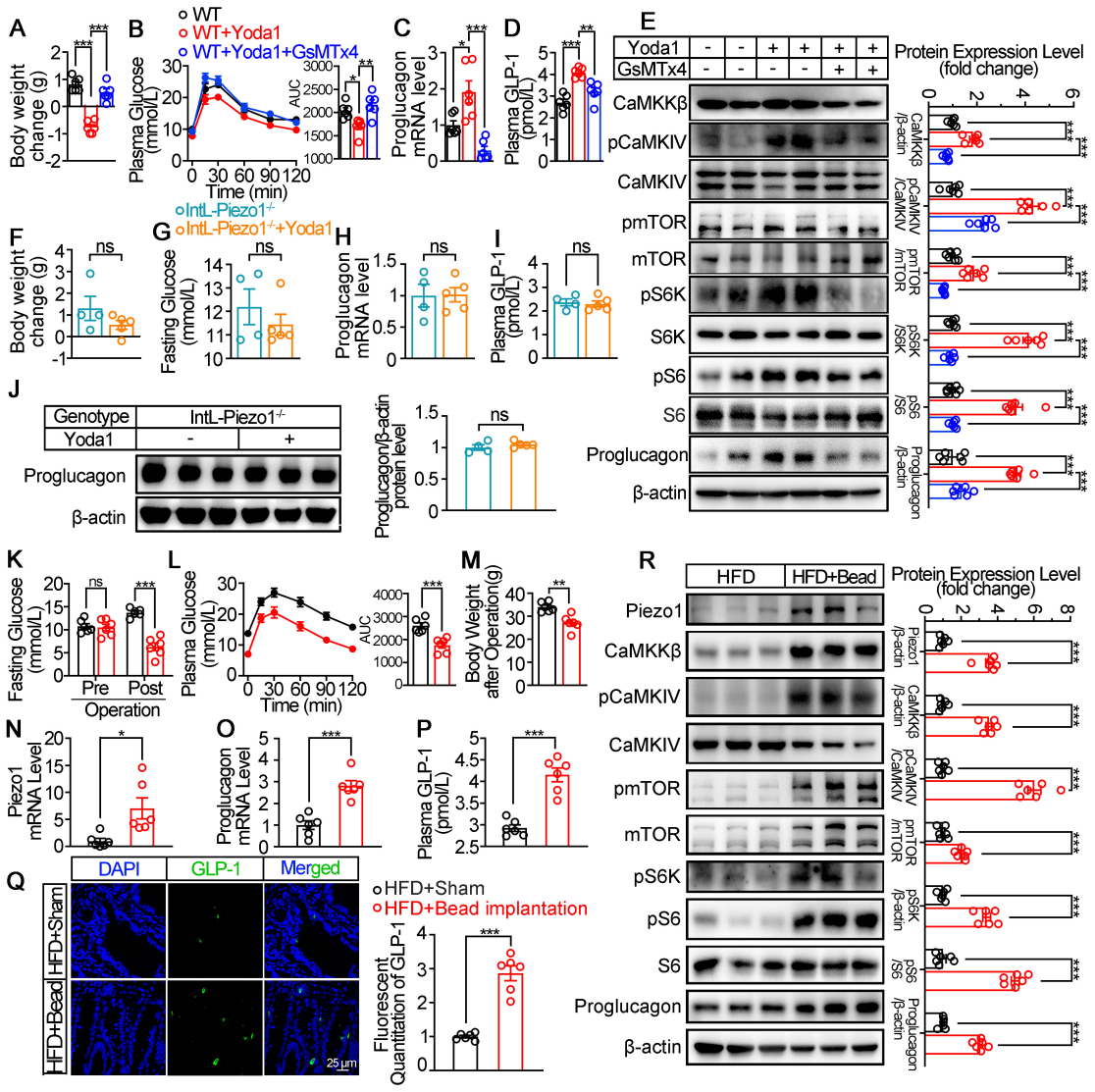
A
Body weight change (g)
B
WT
WT+Yoda1
WT+Yoda1+GsMTx4
Plasma Glucose (mmol/L)
Time (min)
AUC
C
Proglucagon mRNA level
D
Plasma GLP-1 (pmol/L)
E
Yoda1
GsMTx4
Protein Expression Level (fold change)
CaMKKβ
pCaMKIV
CaMKIV
pmTOR
mTOR
pS6K
S6K
pS6
S6
Proglucagon
β-actin
F
Body weight change (g)
G
IntL-Piezo1-/-
IntL-Piezo1-/-+Yoda1
Fasting Glucose (mmol/L)
H
Proglucagon mRNA level
I
Plasma GLP-1 (pmol/L)
J
Genotype
IntL-Piezo1-/-
Yoda1
Proglucagon
β-actin
Proglucagon/β-actin protein level
K
Fasting Glucose (mmol/L)
Pre
Post
Operation
L
Plasma Glucose (mmol/L)
Time (min)
AUC
M
Body Weight after Operation(g)
N
Piezo1 mRNA Level
O
Proglucagon mRNA Level
P
Plasma GLP-1 (pmol/L)
Q
DAPI
GLP-1
Merged
HFD+Sham
HFD+Bead
25 μm
HFD+Sham
HFD+Bead implantation
Fluorescent Quantitation of GLP-1
R
HFD
HFD+Bead
Piezo1

Figure 3

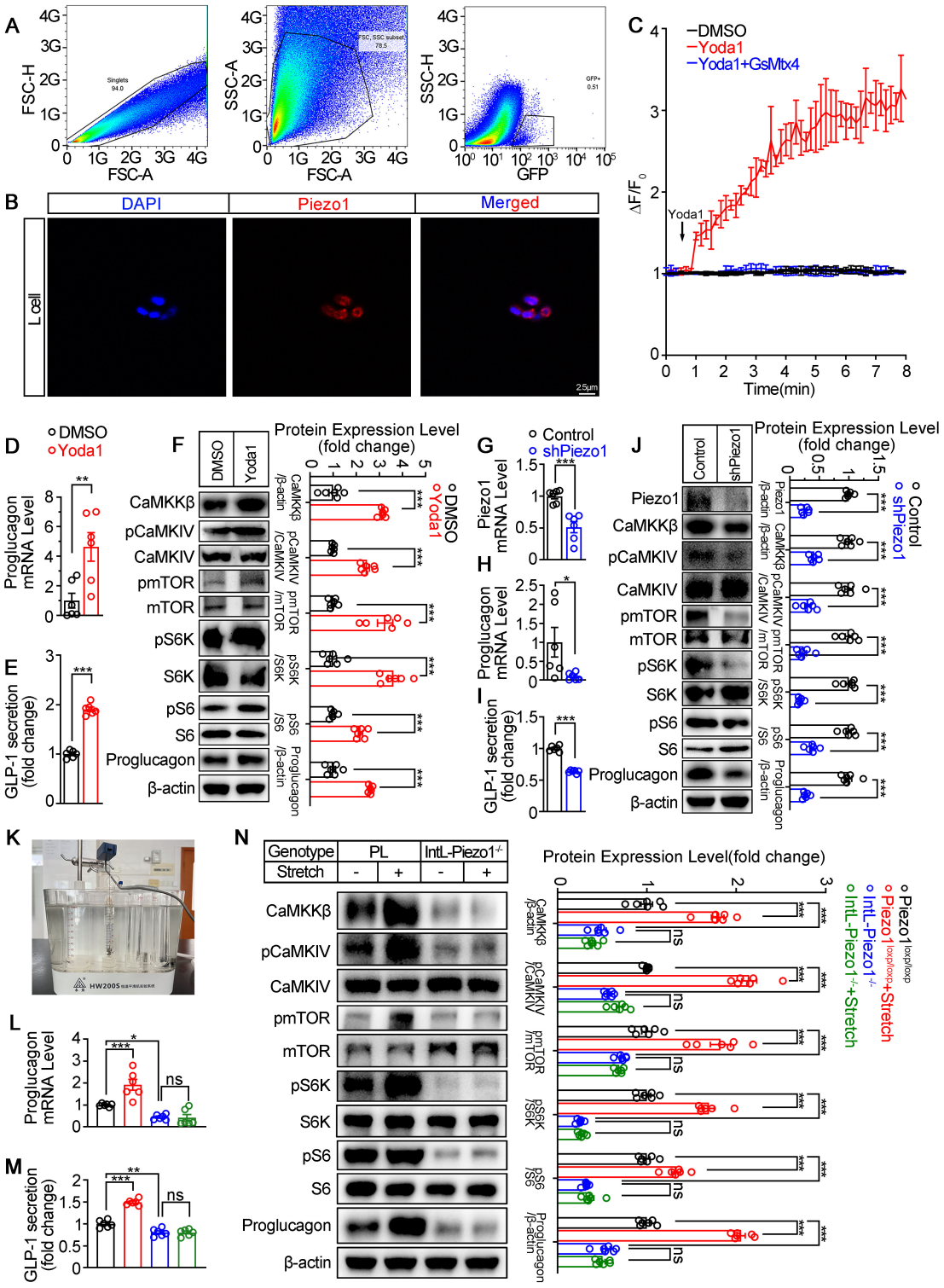
A
FSC-H
FSC-A
SSC-A
SSC-H
GFP
B
DAPI
Piezo1
Merged
L cell
C
DMSO
Yoda1
Yoda1+GsMtx4
ΔF/F0
Time(min)
D
Proglucagon mRNA Level
E
GLP-1 secretion (fold change)
F
Protein Expression Level (fold change)
CaMKKβ
pCaMKIV
CaMKIV
pmTOR
mTOR
pS6K
S6K
pS6
S6
Proglucagon
β-actin
G
Piezo1 mRNA Level
H
I
J
Control
shPiezo1
K
L
M
N
Genotype
PL
IntL-Piezo1-/-
Stretch
Protein Expression Level(fold change)
Piezo1loxp/loxp
Piezo1loxp/loxp+Stretch
IntL-Piezo1-/-
IntL-Piezo1-/-+Stretch

Figure 4

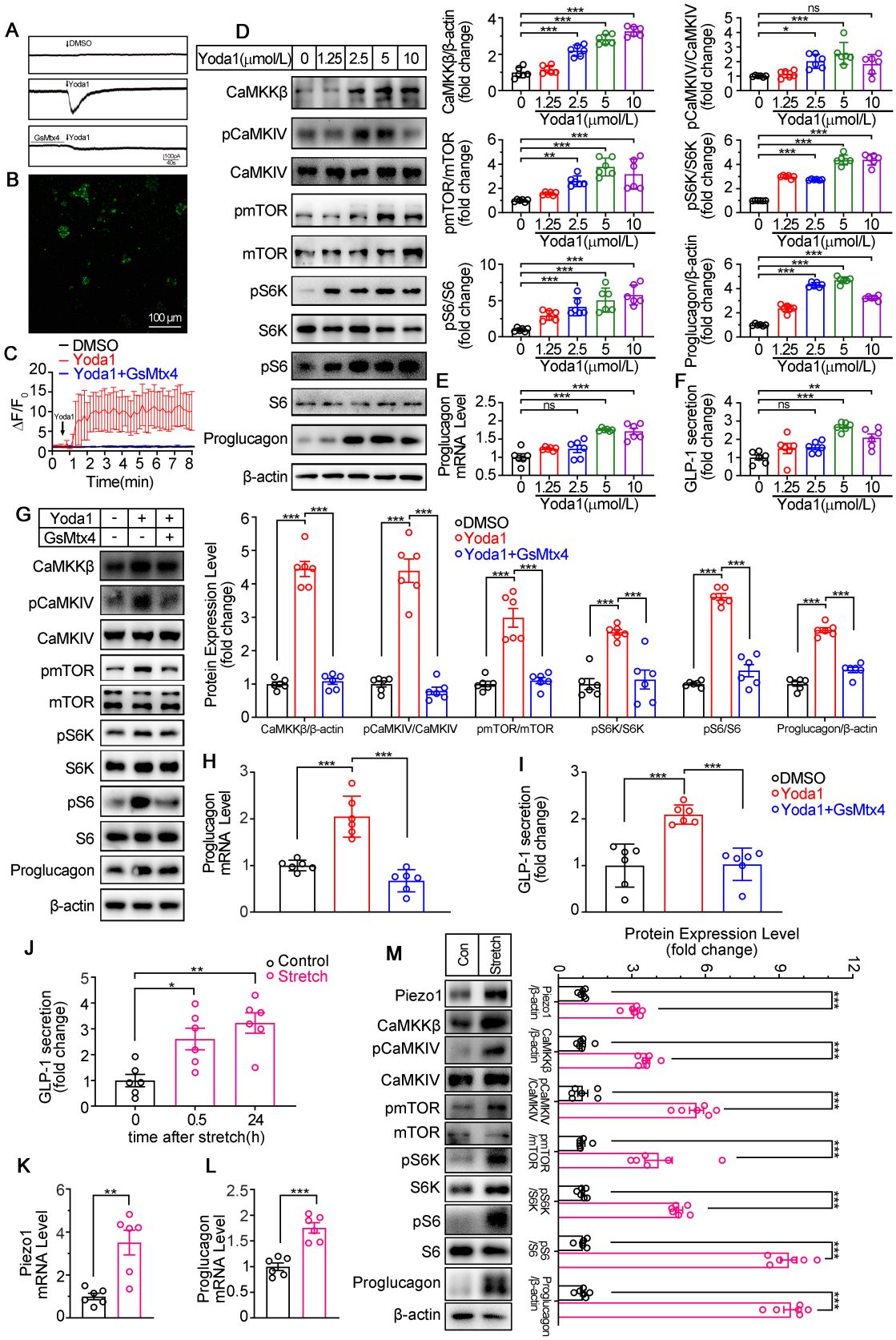
A
DMSO
Yoda1
GsMtx4
B
100 μm
C
DMSO
Yoda1
Yoda1+GsMtx4
ΔF/F0
Time(min)
D
Yoda1(μmol/L)
0
1.25
2.5
5
10
CaMKKβ
pCaMKIV
CaMKIV
pmTOR
mTOR
pS6K
S6K
pS6
S6
Proglucagon
β-actin
CaMKKβ/β-actin (fold change)
pCaMKIV/CaMKIV (fold change)
pmTOR/mTOR (fold change)
pS6K/S6K (fold change)
pS6/S6 (fold change)
Proglucagon/β-actin (fold change)
E
Proglucagon mRNA Level
F
GLP-1 secretion (fold change)
G
Yoda1
GsMtx4
Protein Expression Level (fold change)
CaMKKβ/β-actin
pCaMKIV/CaMKIV
pmTOR/mTOR
pS6K/S6K
pS6/S6
Proglucagon/β-actin
H
I
J
Control
Stretch
time after stretch(h)
K
Piezo1 mRNA Level
L
M
Con
Stretch
Piezo1
Protein Expression Level (fold change)

Figure 5

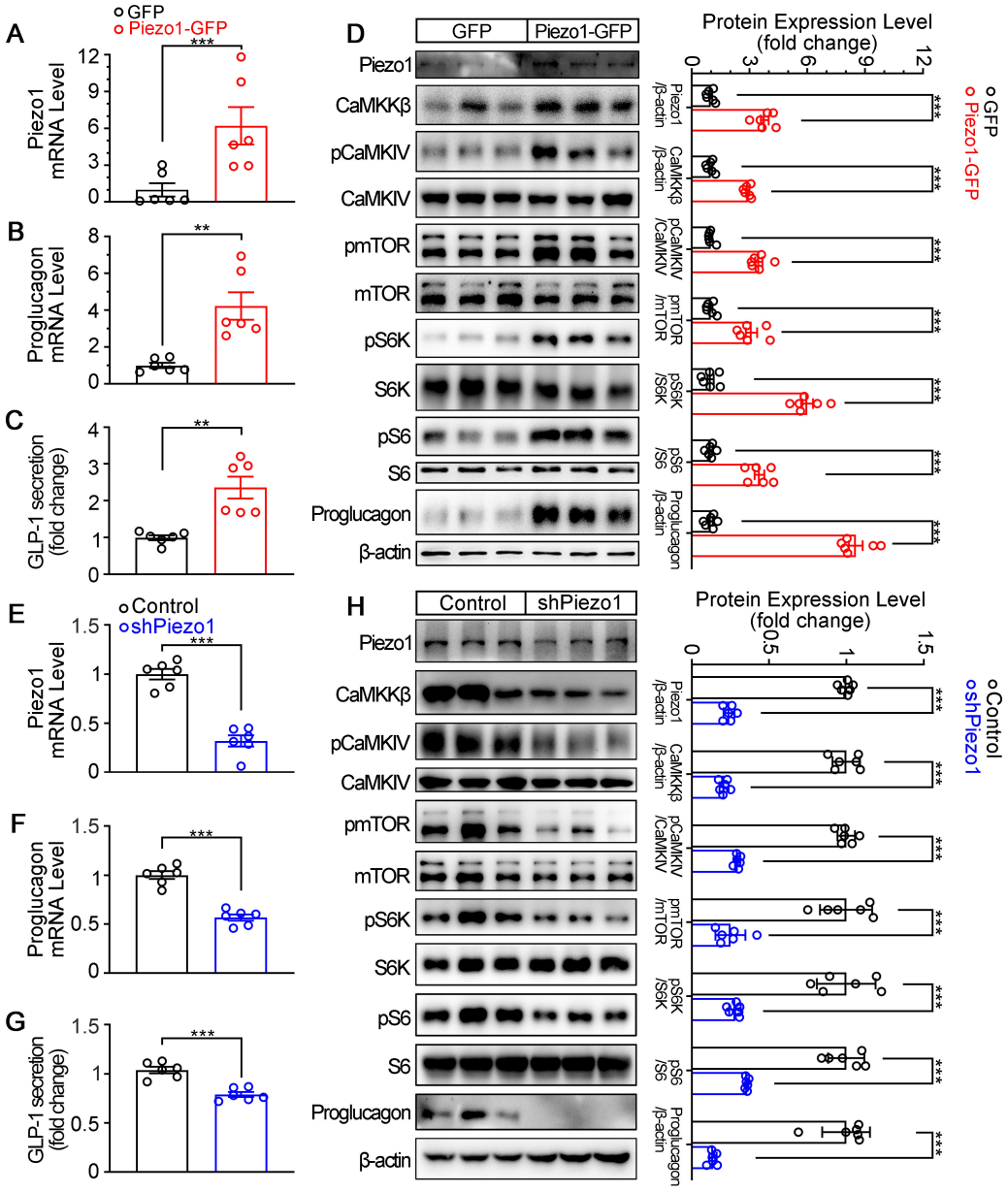
A
GFP
Piezo1-GFP
Piezo1 mRNA Level
B
Proglucagon mRNA Level
C
GLP-1 secretion (fold change)
D
GFP
Piezo1-GFP
Piezo1
CaMKKβ
pCaMKIV
CaMKIV
pmTOR
mTOR
pS6K
S6K
pS6
S6
Proglucagon
β-actin
Protein Expression Level (fold change)
E
Control
shPiezo1
F
G
H

Figure 6

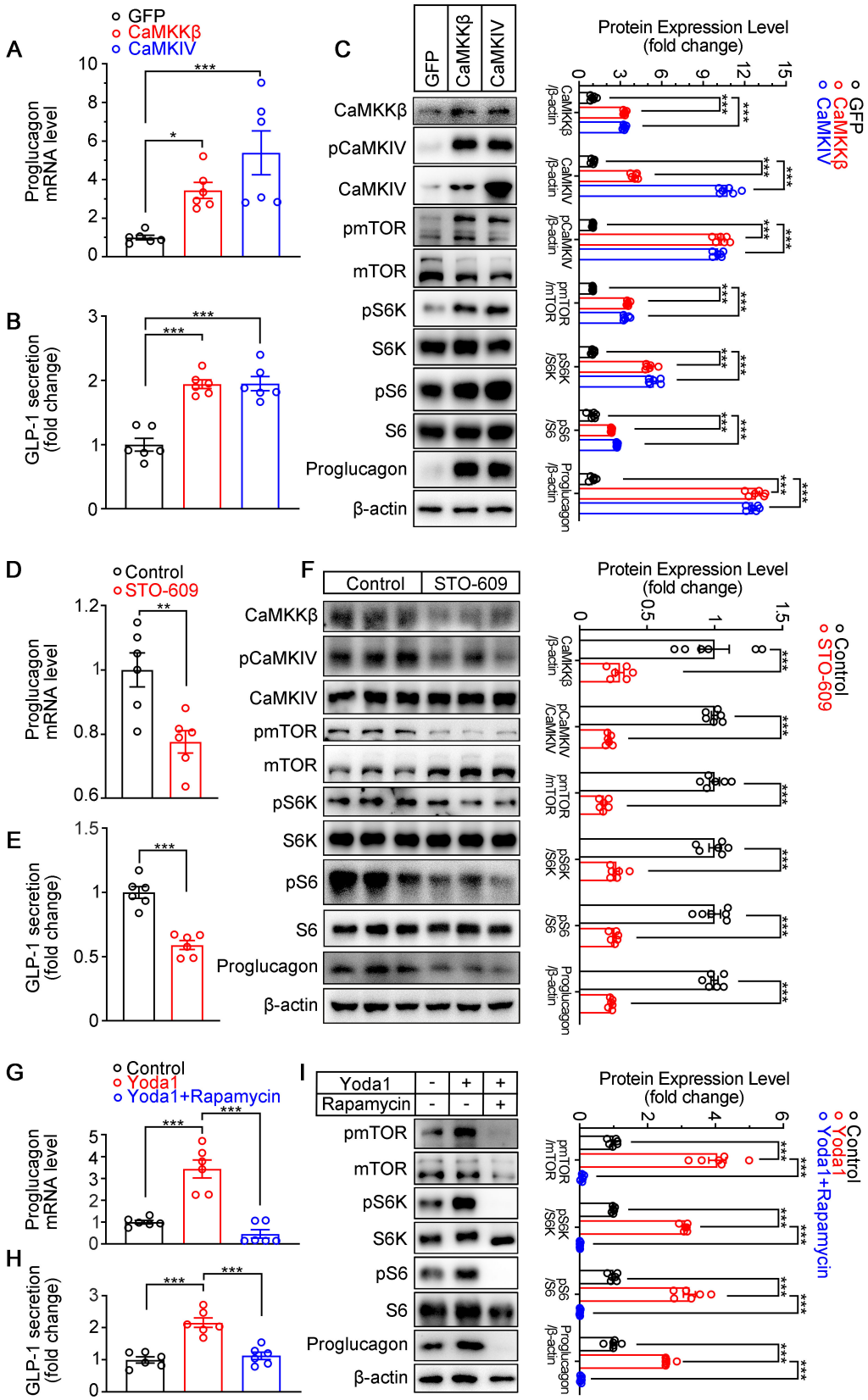
A
GFP
CaMKKβ
CaMKIV
Proglucagon mRNA level
B
GLP-1 secretion (fold change)
C
GFP
CaMKKβ
CaMKIV
CaMKKβ
pCaMKIV
CaMKIV
pmTOR
mTOR
pS6K
S6K
pS6
S6
Proglucagon
β-actin
Protein Expression Level (fold change)
D
Control
STO-609
Proglucagon mRNA level
E
GLP-1 secretion (fold change)
F
Control
STO-609
CaMKKβ
pCaMKIV
CaMKIV
pmTOR
mTOR
pS6K
S6K
pS6
S6
Proglucagon
β-actin
Protein Expression Level (fold change)
G
Control
Yoda1
Yoda1+Rapamycin
Proglucagon mRNA level
H
GLP-1 secretion (fold change)
I
Yoda1
Rapamycin
pmTOR
mTOR
pS6K
S6K
pS6
S6
Proglucagon
β-actin
Protein Expression Level (fold change)

Figure 7